



CENTRO DE INVESTIGACIÓN Y DE ESTUDIOS  
AVANZADOS DEL INSTITUTO POLITECNICO NACIONAL

Unidad Zacatenco

PROGRAMA DE  
SISTEMAS AUTÓNOMOS DE NAVEGACIÓN AÉREA Y  
SUBMARINA

**“Seguimiento de trayectorias utilizando un avión  
miniatura de ala fija”**

TESIS

Que presenta

**HÉCTOR ESCAMILLA NÚÑEZ**

Para obtener el grado de

**MAESTRO EN CIENCIAS**

**EN LA ESPECIALIDAD DE**

**SISTEMAS AUTÓNOMOS DE NAVEGACIÓN AÉREA Y  
SUBMARINA**

**Directores de Tesis:**

**Dr. Rogelio Lozano, Dr. Sergio Salazar.**

**México, D.F.**

**Abril, 2015**



RESEARCH AND ADVANCED STUDIES CENTER  
OF THE NATIONAL POLYTECHNIC INSTITUTE

AERIAL AND SUBMARINE AUTONOMOUS NAVIGATION  
SYSTEMS PROGRAM

**“Path following using a small fixed-wing airplane”**

**HÉCTOR ESCAMILLA NÚÑEZ**

To obtain the degree of

**MASTER IN SCIENCES**

**SPECIALTY IN**

**AERIAL AND SUBMARINE AUTONOMOUS NAVIGATION  
SYSTEMS**

**Thesis supervisors:**

**Ph.D. Rogelio Lozano, Ph.D. Sergio Salazar.**

**Mexico, Mexico city.**

**April, 2015**

## **Acknowledgements.**

To my parents. For their love and steady hand at the right moments that forged in me strength, insight and love.

To my brother. For his limitless support, comprehension and love that only a brother can offer.

To my friends. For their sincere advice full of rawness and truth.

To my cousins. For their simplicity and indiscriminate nobility that makes me love them as brothers.

To my thesis supervisors S. Salazar and R. Lozano, and to G. Flores. For showing me the research environment as well as the different facets and commitments of a researcher.

To CONACyT. For his support program to master students, knowing that without it, the professional and personal growth would have been impossible.

To fate. For encouraging me to personal introspection and search of interior peace.

# Table of Contents.

Resumen. -----	1
Abstract. -----	2
Introduction. -----	4
Objectives. -----	9
Chapter 1. Preliminaries. -----	10
1.1 Notation and Axes. -----	10
1.2 Equations of Motion in the Body Frame.-----	15
1.3 Equations of Motion in the Inertial Frame. -----	18
1.4 Aerodynamic Forces and Moments. -----	19
1.5 Compilation of Equations. -----	22
1.6 Reduced Mathematical Model. -----	25
1.7 Trajectory Parameterization. -----	27
1.8 Serret-Frenet frame. -----	29
Chapter 2. Path Following. -----	34
2.1 First Approach. -----	34
2.2 Second Approach. -----	42
2.2.1 Introduction to Wind Estimation. -----	43
2.2.2 Path Following Model. -----	46
2.2.3 Wind Estimation. -----	49
2.2.4 Path Following Control. -----	51
Chapter 3. Prototype. -----	58
Chapter 4. Results. -----	66
4.1 Simulation Results. -----	66
4.2 Experimental Results. -----	74

Discussion. -----	80
Conclusion. -----	81
Future Work. -----	82
Appendix A. -----	83
Appendix B. -----	86
References. -----	89

# Table of Figures.

## Introduction.

Fig 1 Flying bomb. -----	6
Fig 2 RQ-4 Global Hawk (U.S. UAV). -----	8

## Chapter 1. Preliminaries.

Fig 1.1 Common axe notation and principal forces. -----	11
Fig 1.2 Types of body axes.-----	12
Fig 1.3 Positive sense of angle of attack and angle of sideslip. -----	13
Fig 1.4 Arclength definition. -----	29
Fig 1.5 Circular trajectory parameterized by $\theta$ . -----	31
Fig 1.6 Circular trajectory parameterized by arc length. -----	32

## Chapter 2. Path Following.

Fig 2.1 Diagram for Guidance Logic. -----	36
Fig 2.2 Circular path following. -----	38
Fig 2.3 Wind triangle. -----	43
Fig 2.4 Path Following figure. -----	47
Fig 2.5 Graphic of the term $V e_y \sin \delta(e_y)$ . -----	53
Fig 2.6 Backstepping roll angle simulation. -----	57

## Chapter 3. Prototype.

Fig 3.1 Original airplane. -----	58
Fig 3.2 Modified plane. -----	59
Fig 3.3 Modified airplane (Upper view). -----	59
Fig 3.4 LiPo battery and brushless motor. -----	60
Fig 3.5 Pitot tube. -----	60
Fig 3.6 PX4 autopilot with the expansion ports. -----	61
Fig 3.7 Sensors in the PX4 autopilot. -----	61

Fig 3.8 GPS used. -----	62
Fig 3.9 Frames on earth. -----	63
Fig 3.10 XBee modem. -----	64
Fig 3.11 PX4 autopilot with peripherals and outputs. -----	65

#### Chapter 4. Results.

Fig 4.1 Reference path. -----	66
Fig 4.2 Disturbance in $x$ . -----	67
Fig 4.3 Disturbance in $y$ . -----	68
Fig 4.4 $x$ error in real model. -----	69
Fig 4.5 $x$ error in ideal model. -----	69
Fig 4.6 $y$ error in real model. -----	70
Fig 4.7 $y$ error in ideal model. -----	70
Fig 4.8 $x$ error between real and ideal models. -----	71
Fig 4.9 $y$ error between real and ideal models. -----	71
Fig 4.10 Estimation of the perturbation in $x$ . -----	72
Fig 4.11 Estimation of the perturbation in $y$ . -----	72
Fig 4.12 Plane trajectory. -----	73
Fig 4.13 Trajectory in manual mode. -----	74
Fig 4.14 Trajectory in loiter mode. -----	75
Fig 4.15 Loiter trajectory. -----	76
Fig 4.16 3D trajectory. -----	76
Fig 4.17 Altitude during loiter flight. -----	77
Fig 4.18 Airspeed during partial flight. -----	78
Fig 4.19 Circular trajectory. -----	79

## **Resumen.**

Este trabajo describe dos métodos de seguimiento de trayectorias para aviones miniatura de ala fija.

El primer método cubre el objetivo de tener un algoritmo lo suficientemente preciso y fácil a implementar en una plataforma experimental, este algoritmo muestra tener beneficios sobre métodos lineales para caminos curvos por el hecho de que cuenta con un elemento de anticipación para el camino deseado entrante, con respecto a la orientación en este caso, controladores proporcional-derivativos son utilizados.

Para el segundo método, una encuesta sobre vehículos aéreos no tripulados publicada en 2014, mostró que entre los algoritmos considerados, tales como VF (Vector Field), PLOS (Pure Line of Sight), NLGL (Non Linear Guidance Law) y LQR (Linear Quadratic Regulator), el algoritmo de carrot-chasing, el cual es fácil a implementar, tuvo el peor desempeño debido a su falta de robustez contra perturbaciones de viento, lo cual vislumbra una oportunidad para mejorar las debilidades de este método. Con el fin de hacer una optimización para este tipo de algoritmos contra perturbaciones de viento, y después de la revisión del estado del arte para este tema, un método para estimación de viento es buscado, mas tarde, los resultados son adicionados a un control de posición basado en la teoría de Lyapunov; con respecto a la orientación, un controlador basado en backstepping es propuesto, propiciando un movimiento suave cuando un cambio en la orientación es requerido.

Una visión panorámica de la plataforma experimental así como el hardware utilizado es dada. Finalmente, los resultados, así como el trabajo futuro, son mencionados.



## **Abstract**

This work describes two guidance methods for small fixed-wing airplanes so as to perform path following.

The first approach fulfill the goal of having an algorithm easy to implement in an experimental platform and enough accurate, this method is shown to have a benefit over linear approaches for curved paths, based on the fact that it contains an element of anticipation for the upcoming local desired flight path, concerning to the attitude, a proportional derivative control is used.

For the second approach, a survey of unmanned aerial vehicles published in 2014, showed that among many considered algorithms, such as VF (Vector Field), PLOS (Pure Line of Sight), NLGL (Non Linear Guidance Law) and LQR (Linear Quadratic Regulator), the carrot-chasing algorithm, which is easy to implement, had the worst performance due to the lack of robustness against wind disturbances, which leads to an opportunity to improve the weak points of the method. In order to achieve an optimization for this kind of algorithms considering wind disturbances, and after a revision of the state of art in this subject, a wind estimation method was sought, and then, the results are added to a Lyapunov theory based control for the position; concerning to the attitude, a backstepping approach is proposed, allowing the plane to have a smooth motion when a change of attitude angle is commanded.

A panoramic view of the experimental platform, as well as the hardware used is given. Finally, the results, as well as the expected future work, are mentioned.

## **Abstract**

Ce travail décrit deux méthodes de suivi de trajectoires pour des avions miniatures d'aile-fixée.

La première approche remplit l'objectif d'avoir un algorithme simple à mettre en œuvre sur la plate-forme expérimentale et assez précis, cette méthode est démontrée d'avoir des avantages par rapport aux autres approches linéaires pour des chemins courbes, basée sur le fait qu'il contient un élément de prévision de la prochaine trajectoire voulue locale, concernant à l'orientation du véhicule, une commande proportionnelle- dérivative est utilisée.

Pour la deuxième approche, une enquête sur drones faite en 2014, a montré que parmi quelques algorithmes considérés, tels que VF (Vector Field), PLOS (Pure Line of Sight), NLGL (Non Linear Guidance Law) et LQR (Linear Quadratic Regulator), l'algorithme de carot-chasing, qui est facile à mettre en œuvre, a eu la pire performance à cause de son manque de robustesse contre les perturbations du vent, ce qui conduit à une opportunité d'améliorer les points faibles de la méthode. Afin d'optimiser ce type d'algorithmes contre les perturbations du vent, et après une révision de l'état de l'art dans ce domaine, une méthode pour l'estimation du vent a été cherchée, et puis, les résultats sont ajoutés à une commande basée sur la théorie de Lyapunov pour la position ; concernant à l'orientation, une approche de backstepping est proposée, permettant à l'avion d'avoir un mouvement fluide lors d'un changement de l'angle de roulis est commandée.

Une vue panoramique de la plate-forme expérimentale, ainsi que le matériel utilisé est donnée. Finalement, les résultats, ainsi que le travail futur, sont mentionnés.

## **Introduction.**

Nowadays, society relies more and more on technology when a task is wanted to achieve, this is even more evident when a human being is not able to do tasks as good as a machine or when the presence of a human is endangered due to the environment, which leaves space for a machine to improve the performance. This improvement can be justified by the fact that when a task is asked to a human, there will always be room for danger, fatigue, delays, even a decrease of precision and an increase of time to get the task done.

The context where this work is focused is in the case of a lost person in an unknown area of a forest, where an unmanned airplane is used to find her. In this work is only managed the path following part, but once this problem is solved, a camera or any other sensor can be added to locate the lost person from above, which will close the loop of the final aim of the work. The technique utilized will be a sweep of the area by the airplane, following a desired trajectory which will cover the terrain of interest, it is assumed that all kind of trajectories can be followed using circles and straight lines, where straight lines can be followed with a defined yaw angle, and the circular path, using the proposed methods.

## **Background.**

To begin, some background on airplane's theory extracted from [1][2] is given, then, knowing that path following is used as one of the approaches to follow a trajectory, the geometric path needs to be time-independent, which is why [3] is used to the trajectory reparametrization.

In order to make the airplane to follow a desired trajectory, two different approaches are used in this work.

The first approach, based on [4], and considered as trajectory tracking, gives an algorithm enough accurate and easy to implement in an experimental platform.

The second approach, chosen after the revision of a survey [5] in this domain, is considered as path following. The approach uses a reduced airplane lateral-directional model to describe plane dynamics, given by Dubins [6][7], already utilized in works such as [8][9]. Also, the approach is endowed with a wind estimation algorithm, based on the different methods to manage wind disturbances described in [10] – [17]. It is worth to say that the path following model is based on errors with respect to a virtual target located in the desired trajectory, this idea was introduced in [18]. The mathematical model, very similar to the one used in [19], is utilized to develop a control law based on Lyapunov, like in [20], in order to achieve the path following.

The Unmanned Aerial Vehicles (UAV's), have become a key point of the experimental-theoretical research in a global level, being pioneers the most technologically advanced countries. Actually, UAV's have several applications, going from military to civilian, being the military the most comun.

The first UAV's documented took place on August 22th of 1849, when the Austrian army used unmanned balloons charged with explosives to attack Venice, Italy. However, due to the wind and lack of guidance technology, many balloons failed in their targets.

After the First World War, the concept utilized in Venice was transformed into unmanned bombs, known as "Flying bombs" (see Fig. 1), which consisted of a winged-bomb with a propulsion system, but once again, due to the lack of technology, this improvement was not feasible at large scales.

After some years, in 1917, the U.S. army, created an automatic plane, where the main objective was to make a bomb plane, so it had to be light and economic despite its simple design, this prototype was named as "aerial torpedo", however, it was never used in the war as this ended before the prototype was ready to fly.



Fig. 1: Flying bomb.

It was not until the 30's that an English actor called Reginald Denny, owner of a modeling business and active follower of remote control planes, built a plane for the army which will be a mobile target to train the antiaircraft artillery. During the Second World War were built about 15 thousand copies of this prototype.

The first time a camera was mounted in a plane in order to visualize the transmitted images on a television was until the 40's, time where a significant change in propulsion systems for planes was made, because there were not only the scale piston engine, but also the pulse jet engine.

As time and technology evolved, UAV's did it too, including more and better control techniques, data transmission, electronics, materials, design and many other factors who improved the prototypes.

#### UAV Classification

Nowadays, these vehicles play a key role in several missions due to the advantages they provide, generally, a classification can be made in two groups, the first, by applications, and the second, by altitude/range of operation.

### UAV's by application

- Target: They emulate enemy planes to simulate attacks, this kind is generally used in practical exercises.
- Surveillance and recognition: Vehicles used to transmit information of any kind. Within this category stand out the MUAV's (Micro Unmanned Aerial Vehicle).
- Combat: designed to attack or support an attack on combat missions, known asUCAV (Unmanned Combat Air Vehicle).
- Logistics: Built to transport load.
- Research: New systems of any kind are developed in them.
- Civilian: Designed to develop scientific research, disaster support and civilian surveillance.

### UAV's by altitude/range of operation

- Handheld: Operation at 2,000 ft height, until 2 km of reach.
- Close: Operation at 5,000 ft height, until 10 km of reach.
- NATO: Operation at 10,000 ft height, until 50 km of reach.
- Tactical: Operation at 18000 ft height, until 160 km of reach.
- MALE (medium altitude, long endurance): Operation at 30,000 ft height and until 200 km of reach.
- HALE (high altitude, long endurance): Operation at 30,000 ft and undetermined reach.
- HYPERSONIC: High speed UAV, supersonic (Mach 1-5) or hypersonic (Mach 5+), operation at 50,000 ft or suborbital height, reach of 200km.
- ORBITAL: Operation at low terrestrial orbits (Mach 25+).
- CIS Lunar: Perform travels between the Moon and the Earth.

The Fig. 2 shows an HALE UAV approved by the Federal Aviation Administration since 2003, which can perform 36 hours of continuous flight at 18,300 m height and 635 km per hour as maximum speed.



Fig. 2: RQ-4 Global Hawk (U.S. UAV).

## **Objectives.**

### Main Objectives

- To find the mathematical equations that define the behavior of a plane.
- To find the main aerodynamic forces and moments equations in the plane model.
- To find a path following algorithm easy to implement in an experimental platform.
- To obtain experimental results of the implemented algorithm.

### Secondary objectives

- To propose an algorithm with robustness against wind disturbances.
- To perform the simulations of the proposed robust control.
- To implement and obtain experimental data of the robust control.



# Chapter 1.

## Preliminaries.

In this part, the principal notation, aerodynamic forces and moments, as well as the main reduced equations of motion of the plane are presented, furthermore, and knowing that one of the control strategies uses path following, some reparametrization theory is given in order to obtain a time-independent path.

### 1.1 Notation and Axes

According to reference [1], the earth is assumed as a flat surface and as the inertial reference frame. The frame's origin is arbitrarily located and will be denoted by  $F_E(O_E, x_E, y_E, z_E)$ , where the  $z_E$  axe points downwards, also, the gravity field is considered uniform everywhere.

The plane's gravity center (CG) and mass center are located at the same point, the plane velocity  $V_E$ , expressed in  $F_E$ , is the groundspeed, however, aerodynamic forces and moments are not dependent on groundspeed, they depend on the air mass that surrounds the plane called airspeed, which will vary when wind is present. The wind velocity in the inertial frame is denoted as  $W$ , and relative velocity of CG to the air as  $V$ , then:

$$V_E = V + W$$

Where the components of the wind in  $F_E$  will be given by

$$W_E = \begin{bmatrix} W_{x_E} & W_{y_E} & W_{z_E} \end{bmatrix}^T$$

A second reference frame, attached to the body's CG, is defined as  $F_B(C, x, y, z)$ , and referred to it as the body axes. A symmetry plane  $Cxz$  will be chosen to simplify mathematical equations; main moments and aerodynamic forces as well as common notation are shown in the Fig. 3.

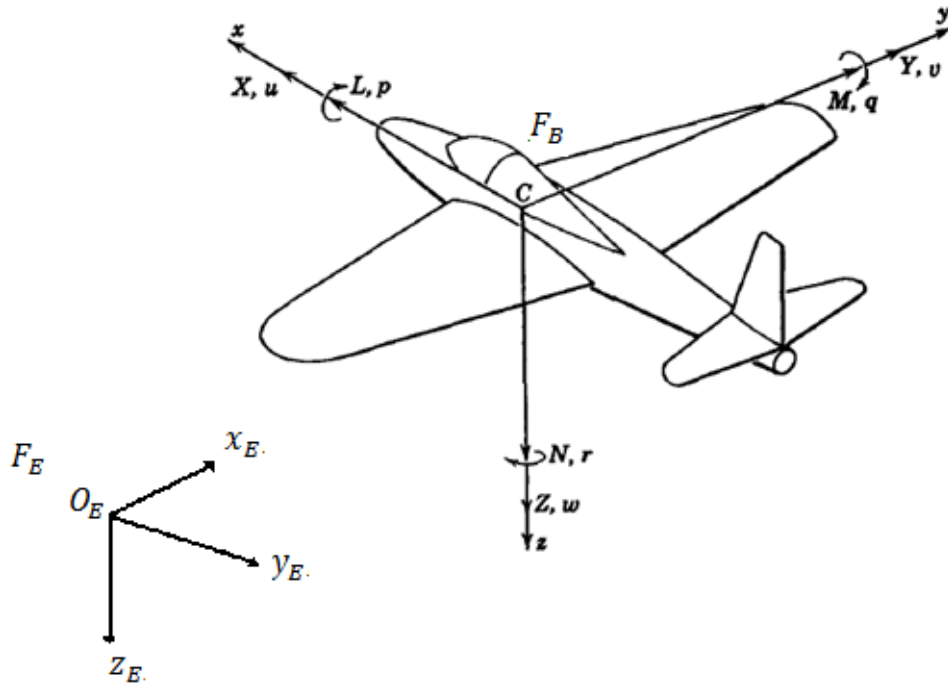


Fig. 1.1: Common axe notation and principal forces.

According to the Fig. 1.1, the following notation is adopted:

$L$	Rolling moment
$M$	Pitching moment
$N$	Yawing moment
$p$	Roll rate
$q$	Pitch rate
$r$	Yaw rate
$[X, Y, Z]$	Resultant aerodynamic force components
$[u, v, w]$	Components of velocity of CG relative to surrounding air mass
$V_B = [u \ v \ w]^T$	Aircraft velocity expressed in the body frame

It is worth to say that the aerodynamic forces of the plane, caused by  $V$ , are generated in the wind frame, that is a different frame than the body frame, due to this, three more frames are explained in order to make the optimal choice of body axes.

### Principal Axes.

These axes, denoted by  $F_P(C, x_P, y_P, z_P)$ , together with the symmetry plane  $Cxz$ , are chosen wisely in order to make the inertia product  $I_{zx}$  to disappear.

### Stability axes.

These axes, defined as  $F_S(C, x_S, y_S, z_S)$ , are chosen for  $Cx$  to be aligned with  $V$  in a continuous symmetric flight. In this case,  $v$  and  $w$  are zero, but as the wind changes, the axes orientation relative to the plane also changes, which leads to a changing inertia matrix. The Fig. 1.2, represent the relation between these axes, where  $\epsilon$  is the angle between principal axes (denoted by subindex  $P$ ) and stability axes (denoted by subindex  $S$ ).

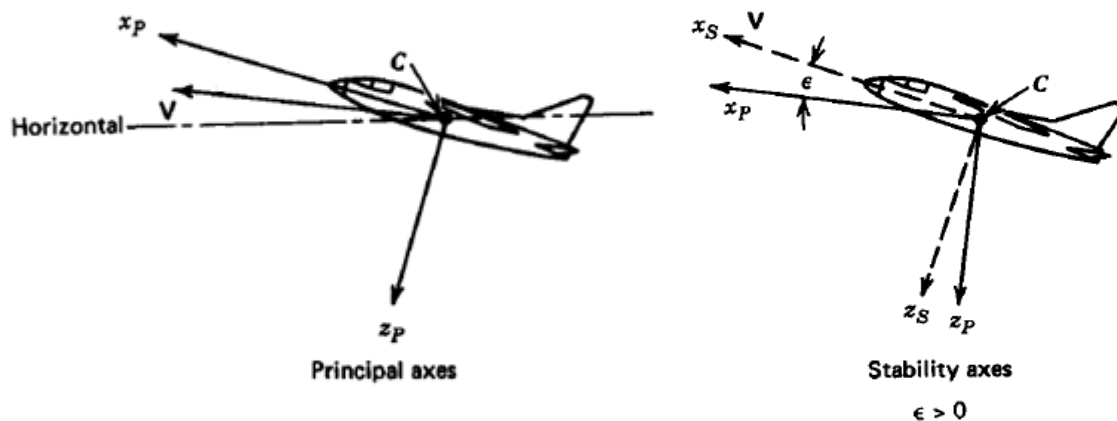


Fig. 1.2: Types of body axes.

### Wind axes.

These axes are completely parallel to the wind, so that the wind only has one component in this frame, which is where the aerodynamic forces are generated, but as the wind is unknown and shifting, the wind in the body axes can be expressed using a simple rotation matrix around two axes detailed as follows:

$$\begin{bmatrix} x \\ y \\ z \end{bmatrix}_{stab} = \begin{bmatrix} \cos \alpha & 0 & -\sin \alpha \\ 0 & 1 & 0 \\ \sin \alpha & 0 & \cos \alpha \end{bmatrix} \begin{bmatrix} x \\ y \\ z \end{bmatrix}_{body}$$

$$\begin{bmatrix} x \\ y \\ z \end{bmatrix}_{wind} = \begin{bmatrix} \cos \beta & \sin \beta & 0 \\ -\sin \beta & \cos \beta & 0 \\ 0 & 0 & 1 \end{bmatrix} \begin{bmatrix} x \\ y \\ z \end{bmatrix}_{stab}$$

So, knowing that the velocity of CG expressed in the wind axes has by definition only the component of the airspeed vector,  $V_{wind} = [V \ 0 \ 0]^T$  and using the rotation matrix  $S_{WB}$ , which is the matrix to express the body axes in the wind axes:

$$V_{wind} = S_{WB} V_{body}$$

$$S_{WB} = \begin{bmatrix} \cos \beta & \sin \beta & 0 \\ -\sin \beta & \cos \beta & 0 \\ 0 & 0 & 1 \end{bmatrix} \begin{bmatrix} \cos \alpha & 0 & -\sin \alpha \\ 0 & 1 & 0 \\ \sin \alpha & 0 & \cos \alpha \end{bmatrix} = \begin{bmatrix} \cos \alpha \cos \beta & \sin \beta & \sin \alpha \cos \beta \\ -\cos \alpha \sin \beta & \cos \beta & -\sin \alpha \sin \beta \\ -\sin \alpha & 0 & \cos \alpha \end{bmatrix}$$

It leads to

$$V_B = \begin{bmatrix} u \\ v \\ w \end{bmatrix} = S_{WB}^T V_{wind} = S_{BW} \begin{bmatrix} V \\ 0 \\ 0 \end{bmatrix}$$

$$\begin{bmatrix} u \\ v \\ w \end{bmatrix} = \begin{bmatrix} V \cos \alpha \cos \beta \\ V \sin \beta \\ V \sin \alpha \cos \beta \end{bmatrix} \quad |V| = (u^2 + v^2 + w^2)^{\frac{1}{2}}$$

Where  $\alpha$  is the angle of attack, and  $\beta$  the angle of sideslip, given by the relations (see Fig. 1.3):

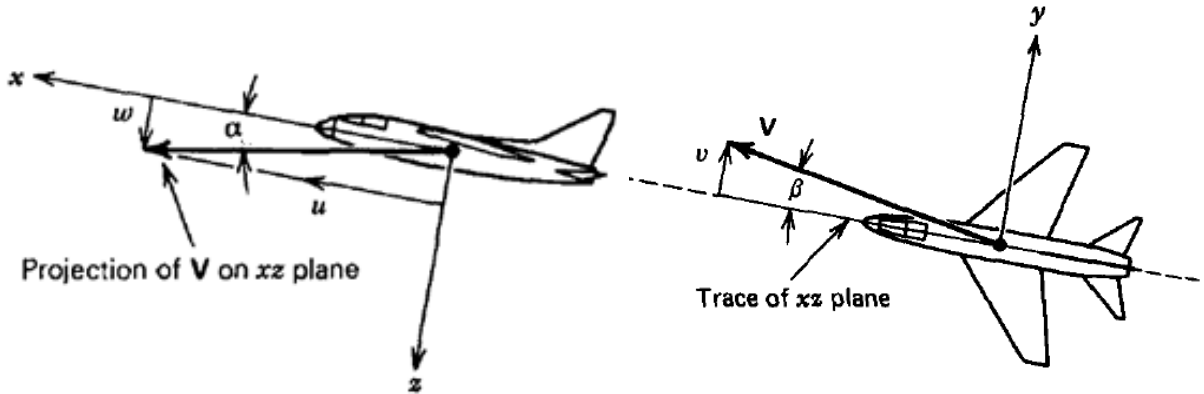


Fig. 1.3: Positive sense of angle of attack and angle of sideslip.

$$\alpha = \tan^{-1} \frac{w}{u} \qquad \beta = \sin^{-1} \frac{u}{v}$$

The movement of the airplane will be described by the Euler's angles

$$\Omega = [\phi \ \theta \ \psi]^T$$

In order to avoid singularities, they are bounded as follows:

$$-180^\circ < \psi < 180^\circ \quad \text{or} \quad 0 < \psi < 360^\circ$$

$$-90^\circ < \theta < 90^\circ$$

$$-180^\circ < \phi < 180^\circ \quad \text{or} \quad 0 < \phi < 360^\circ$$

Furthermore, the rotation matrix from the body frame to the inertial frame, based on Euler's angles, considering a rotation around the axis in the order  $zyx$ , is given by:

$$L_{EB} = \begin{bmatrix} \cos \theta \cos \psi & \sin \phi \sin \theta \cos \psi - \cos \phi \sin \psi & \cos \phi \sin \theta \cos \psi + \sin \phi \sin \psi \\ \cos \theta \sin \psi & \sin \phi \sin \theta \sin \psi + \cos \phi \cos \psi & \cos \phi \sin \theta \sin \psi - \sin \phi \cos \psi \\ -\sin \theta & \sin \phi \cos \theta & \cos \phi \cos \theta \end{bmatrix}$$

Then, the groundspeed is considered as  $V_E = [x_E \ y_E \ z_E]^T$  along with the velocity in the body frame, the rotation matrix with the wind taken into account (see Fig. 10) will lead to the expression:

$$V_E = L_{EB}V_B + W_E$$

Therefore, it can be expressed as follows:

$$\begin{bmatrix} \dot{x}_E \\ \dot{y}_E \\ \dot{z}_E \end{bmatrix} = \begin{bmatrix} \cos \theta \cos \psi & \sin \phi \sin \theta \cos \psi - \cos \phi \sin \psi & \cos \phi \sin \theta \cos \psi + \sin \phi \sin \psi \\ \cos \theta \sin \psi & \sin \phi \sin \theta \sin \psi + \cos \phi \cos \psi & \cos \phi \sin \theta \sin \psi - \sin \phi \cos \psi \\ -\sin \theta & \sin \phi \cos \theta & \cos \phi \cos \theta \end{bmatrix} \begin{bmatrix} u \\ v \\ w \end{bmatrix} + \begin{bmatrix} W_{x_E} \\ W_{y_E} \\ W_{z_E} \end{bmatrix}$$

The angular velocity, which takes place in the body frame  $\omega_B = [p \ q \ r]^T$  will hold the following relation with the Euler's angles

$$\omega_B = \begin{bmatrix} p \\ q \\ r \end{bmatrix} = R \begin{bmatrix} \dot{\phi} \\ \dot{\theta} \\ \dot{\psi} \end{bmatrix} = R\dot{\Omega}$$

Where:

$$R = \begin{bmatrix} 1 & 0 & -\sin \theta \\ 0 & \cos \phi & \cos \theta \sin \phi \\ 0 & -\sin \phi & \cos \theta \cos \phi \end{bmatrix}$$

Leading to:

$$\begin{bmatrix} p \\ q \\ r \end{bmatrix} = \begin{bmatrix} \dot{\phi} - \dot{\psi} \sin \theta \\ \dot{\theta} \cos \phi + \dot{\psi} \cos \theta \sin \phi \\ -\dot{\theta} \sin \phi + \dot{\psi} \cos \theta \cos \phi \end{bmatrix}$$

Then, expressing the inverse relation:

$$\dot{\Omega} = \begin{bmatrix} \dot{\phi} \\ \dot{\theta} \\ \dot{\psi} \end{bmatrix} = T \begin{bmatrix} p \\ q \\ r \end{bmatrix} = T\omega_B$$

$$T = R^{-1} = \begin{bmatrix} 1 & \sin \phi \tan \theta & \cos \phi \tan \theta \\ 0 & \cos \phi & -\sin \phi \\ 0 & \sin \phi \sec \theta & \cos \phi \sec \theta \end{bmatrix}$$

$$\begin{bmatrix} \dot{\phi} \\ \dot{\theta} \\ \dot{\psi} \end{bmatrix} = \begin{bmatrix} p + (q \sin \phi + r \cos \phi) \tan \theta \\ q \cos \phi - r \sin \phi \\ (q \sin \phi + r \cos \phi) \sec \theta \end{bmatrix}$$

## 1.2 Equations of Motion in the Body Frame.

Using the Euler's approach considering  $f$  as the external forces,  $A_B = [X \ Y \ Z]^T$  as the aerodynamic forces,  $g$  as the gravity with only a vertical component in the inertial frame, and using the property

$$\begin{aligned} \dot{L}_{BE} &= -\tilde{\omega}_B L_{BE} \\ \dot{L}_{BE}^T &= (-\tilde{\omega}_B L_{BE})^T \\ \dot{L}_{EB} &= (L_{BE})^T (-\tilde{\omega}_B)^T \\ \dot{L}_{EB} &= L_{EB} \tilde{\omega}_B \end{aligned}$$

Where  $\tilde{\omega}_B$  is the skew symmetric matrix:

$$\tilde{\omega}_B = \begin{bmatrix} 0 & -r & q \\ r & 0 & -p \\ -q & p & 0 \end{bmatrix}$$

The equations expressed in the body frame taking the wind into account like in [13], can be described as:

$$\begin{aligned} f_E &= m\dot{V}_E \\ f_E &= L_{EB}f_B = m \frac{d}{dt} (L_{EB}V_B + W_E) = m(L_{EB}\dot{V}_B + \dot{L}_{EB}V_B + \dot{W}_E) \\ L_{EB}f_B &= m(L_{EB}\tilde{\omega}_B V_B + L_{EB}\dot{V}_B + \dot{W}_E) \end{aligned}$$

Multiplying both sides by  $L_{BE}$  :

$$f_B = m(\dot{V}_B + \tilde{\omega}_B V_B + L_{BE}\dot{W}_E)$$

The vector of external forces  $f_B$  is defined as the sum of the aerodynamic forces  $A_B = [X \ Y \ Z]^T$  and the gravitational force in the body frame, it means:

$$f_B = mL_{BE} \begin{bmatrix} 0 \\ 0 \\ g \end{bmatrix} + \begin{bmatrix} X \\ Y \\ Z \end{bmatrix}$$

Then mixing these latter equations, it is obtained:

$$\begin{bmatrix} X - mg \sin \theta \\ Y + mg \cos \theta \sin \phi \\ Z + mg \cos \theta \cos \phi \end{bmatrix} = m \begin{bmatrix} \dot{u} + qw - rv \\ \dot{v} + ru - pw \\ \dot{w} + pv - qu \end{bmatrix} + mL_{BE}\dot{W}_E$$

Therefore, when the expression is expanded

$$\begin{aligned}
 X - mg \sin \theta &= m(\dot{u} + qw - rv) + W_{x_E} \cos \theta \cos \psi + W_{y_E} \cos \theta \sin \psi - W_{z_E} \sin \theta \\
 & \\
 Y + mg \cos \theta \sin \phi & \\
 &= m(\dot{v} + ru - pw) + W_{x_E} (\sin \phi \sin \theta \cos \psi - \cos \phi \sin \psi) \\
 &+ W_{y_E} (\sin \phi \sin \theta \sin \psi + \cos \phi \cos \psi) + W_{z_E} \sin \phi \cos \theta \\
 & \\
 Z + mg \cos \theta \cos \phi & \\
 &= m(\dot{w} + pv - qu) + W_{x_E} (\cos \phi \sin \theta \cos \psi + \sin \phi \sin \psi) \\
 &+ W_{y_E} (\cos \phi \sin \theta \sin \psi - \sin \phi \cos \psi) + W_{z_E} \cos \phi \cos \theta
 \end{aligned}$$

Following a similar method, considering the aerodynamic moments  $G_E$  expressed in the body frame as  $G_B = [L \quad M \quad N]^T$ , and assuming that the inertia matrix  $I_B$  is given by the components in the diagonal due to the symmetrical plane  $xz$  (making  $I_{xy} = I_{yz} = 0$ , and with the term  $I_{zx}$  neglected),

$$I_B = \begin{bmatrix} I_x & 0 & 0 \\ 0 & I_y & 0 \\ 0 & 0 & I_z \end{bmatrix}$$

Its derivative as zero for being a rigid body ( $\dot{I}_B = 0$ ), and the angular momentum  $h_E$  with respect to  $CG$  of the plane and its expression in the body frame as  $h_B = I_B \omega_B$ , it is obtained.

$$G_E = \dot{h}_E$$

$$G_E = L_{EB} G_B = \frac{d}{dt} (L_{EB} h_B) = \dot{L}_{EB} h_B + L_{EB} \dot{h}_B$$

$$L_{EB} G_B = L_{EB} \tilde{\omega}_B h_B + L_{EB} \dot{h}_B$$

Multiplying both sides by  $L_{BE}$  :

$$G_B = \dot{h}_B + \tilde{\omega}_B h_B$$

$$G_B = \dot{I}_B \omega_B + I_B \dot{\omega}_B + \tilde{\omega}_B I_B \omega_B = I_B \dot{\omega}_B + \tilde{\omega}_B I_B \omega_B$$



Rearranging this expression to matrix form, it leads to.

$$\begin{bmatrix} L \\ M \\ N \end{bmatrix} = \begin{bmatrix} I_x & 0 & 0 \\ 0 & I_y & 0 \\ 0 & 0 & I_z \end{bmatrix} \begin{bmatrix} \dot{p} \\ \dot{q} \\ \dot{r} \end{bmatrix} + \begin{bmatrix} 0 & -r & q \\ r & 0 & -p \\ -q & p & 0 \end{bmatrix} \begin{bmatrix} I_x & 0 & 0 \\ 0 & I_y & 0 \\ 0 & 0 & I_z \end{bmatrix} \begin{bmatrix} p \\ q \\ r \end{bmatrix}$$

Therefore:

$$L = I_x \dot{p} - (I_y - I_z)qr$$

$$M = I_y \dot{q} - (I_z - I_x)rp$$

$$N = I_z \dot{r} - (I_x - I_y)pq$$

### 1.3 Equations of Motion in the Inertial Frame.

Using the expressions given above with the rotation matrix  $L_{EB}$  to express the body axes in the inertial axes, with  $\dot{V}_E = [\dot{x}_E \ \dot{y}_E \ \dot{z}_E]^T$ , the equations of motion are denoted by functions of the aerodynamic moments and forces, and expressed in the inertial frame with an inertia matrix reduced are:

$$\begin{aligned} m\ddot{x}_E &= X \cos \theta \cos \psi + Y(\sin \phi \sin \theta \cos \psi - \cos \phi \sin \psi) \\ &\quad + Z(\cos \phi \sin \theta \cos \psi + \sin \phi \sin \psi) \end{aligned}$$

$$\begin{aligned} m\ddot{y}_E &= X \cos \theta \sin \psi + Y(\sin \phi \sin \theta \sin \psi + \cos \phi \cos \psi) \\ &\quad + Z(\cos \phi \sin \theta \sin \psi - \sin \phi \cos \psi) \end{aligned}$$

$$m\ddot{z}_E = mg - X \sin \theta + Y \sin \phi \cos \theta + Z \cos \phi \cos \theta$$

$$\begin{aligned} L &= I_y(\dot{\theta} \sin \phi - \dot{\psi} \cos \theta \cos \phi)(\dot{\theta} \cos \phi + \dot{\psi} \cos \theta \sin \phi) \\ &\quad + I_z(\dot{\theta} \cos \phi + \dot{\psi} \cos \theta \sin \phi)(-\dot{\theta} \sin \phi + \dot{\psi} \cos \theta \cos \phi) \\ &\quad + I_x(\ddot{\theta} - \ddot{\psi} \sin \theta - \dot{\psi} \dot{\theta} \cos \theta) \end{aligned}$$

$$\begin{aligned}
 M = & I_x(-\dot{\theta} \sin \phi + \dot{\psi} \cos \theta \cos \phi)(\dot{\phi} - \dot{\psi} \sin \theta) \\
 & + I_z(\dot{\psi} \sin \theta - \dot{\phi})(-\dot{\theta} \sin \phi + \dot{\psi} \cos \theta \cos \phi) \\
 & + I_y(\ddot{\theta} \cos \phi + \ddot{\psi} \cos \theta \sin \phi - \dot{\phi} \dot{\theta} \sin \phi \\
 & + \dot{\psi}(\dot{\phi} \cos \theta \cos \phi - \dot{\theta} \sin \theta \sin \phi))
 \end{aligned}$$

$$\begin{aligned}
 N = & I_x(-\dot{\theta} \cos \phi - \dot{\psi} \cos \theta \sin \phi)(\dot{\phi} - \dot{\psi} \sin \theta) \\
 & + I_y(\dot{\phi} - \dot{\psi} \sin \theta)(\dot{\theta} \cos \phi + \dot{\psi} \cos \theta \sin \phi) + I_z(-\ddot{\theta} \sin \phi + \ddot{\psi} \cos \theta \cos \phi \\
 & - \dot{\phi} \dot{\theta} \cos \phi - \dot{\psi}(\dot{\phi} \cos \theta \sin \phi + \dot{\theta} \sin \theta \cos \phi))
 \end{aligned}$$

## 1.4 Aerodynamic Forces and Moments.

According to [2], aerodynamic forces and moments are dependent in part on rotational velocities, deflection of control surfaces, wind velocity, wind direction, plane velocity, air density, and certain coefficients described below. The flight conditions are never the same, that is why nonlinear functions involving variables such as Mach number, attack and sideslip angles, altitude, are used, but in order to avoid this functions, certain coefficients already tested in wind tunnels are defined and applied under certain conditions.

The resultant external force acting on a plane can be decomposed in lift and drag, forces which increase their magnitude as well as the angle of attack and/or the airspeed increase, without reaching certain limit that induces a stall phenomenon.

Lift and drag forces are supposed to be in the wing's pressure center, so that if a frame has its origin in this point of the plane, the pitch moment is equal to zero. This decision is far from being the optimal due to the changing location of the pressure center along the wing as the angle of attack changes. In order to avoid this problem, a point called aerodynamic center is defined. In the aerodynamic center, the pitch moment is almost invariant relative to the angle of attack variation (within permitted limits), for this reason, the CG of the plane is sought to be in this point.

Nevertheless, in subsonic velocities ( $Ma < 1$ ), the aerodynamic center is at  $\frac{1}{4}$  of the wing chord, that is geometrically forward the pressure center, causing by definition a nose-down moment approximately constant relative to the attack angle variation if a frame is chosen with an origin in the aerodynamic center.

The principal aerodynamic forces and moments can be denoted in the wind frame by:

$$D = \bar{q}SC_D \quad \text{Drag force}$$

$$\bar{L} = \bar{q}SC_L \quad \text{Lift force}$$

$$\bar{Y} = \bar{q}SC_Y \quad \text{Lateral force}$$

$$L' = \bar{q}SbC_l \quad \text{Rolling moment}$$

$$M' = \bar{q}S\bar{c}C_m \quad \text{Pitching moment}$$

$$N' = \bar{q}SbC_n \quad \text{Yawing moment}$$

Where:

$$\bar{q} = \frac{1}{2}\rho V^2 = \text{Dynamic pressure}$$

(Models the way in which moments and forces depend on airspeed and air density)

$$\rho = \text{Air density}$$

$$V = \text{Airspeed}$$

$$S = \text{Wing area}$$

$$b = \text{Wingspan}$$

$$\bar{c} = \text{Geometric mean of the wing chord}$$

$$C_D = \text{Drag coefficient}$$

$$C_L = \text{Lift coefficient}$$

$$C_Y = \text{Lateral force coefficient}$$

$$C_l = \text{Rolling coefficient}$$

$C_m$  = Pitching coefficient

$C_n$  = Yawing coefficient

These aerodynamic coefficients can be extracted from already tested airfoils, reported by the *National Advisory Committee for Aeronautics (NACA)*, in documents such as the Technical Report 93 “Aerodynamic characteristics of Airfoils” or the Technical Report 824 “Summary of Airfoil Data”, furthermore, there also exist software to calculate these coefficients like *XFOIL*, which is an interactive program for the design and analysis of subsonic isolated airfoils, moreover, information about these coefficients can be found in the chapter 2 (subsections 2.2 and 2.3) of reference [2].

Also, the thrust due to the motor ( $T_{th}$ ), is a force that depends on its rotation multiplied with a gain  $T_{th} = K_M \omega_M^2$  and should be added in the equations of aerodynamic forces and moments given by

$$A_B = \begin{bmatrix} X \\ Y \\ Z \end{bmatrix} = A_{Baerod} + A_{Bthrust}$$

Knowing that the forces are in the wind frame:

$$A_W = S_{WB} A_B = S_{WB} A_{Baerod} + S_{WB} A_{Bthrust}$$

$$A_W = \begin{bmatrix} -D \\ \bar{Y} \\ -\bar{L} \end{bmatrix} + S_{WB} \begin{bmatrix} T_{th} \\ 0 \\ 0 \end{bmatrix}$$

Expressing these forces in the body frame using the rotation matrix to go from the wind axes to the body axes:

$$\begin{bmatrix} X \\ Y \\ Z \end{bmatrix} = S_{BW} \begin{bmatrix} -D \\ \bar{Y} \\ -\bar{L} \end{bmatrix} + A_{Bthrust}$$

$$\begin{bmatrix} X \\ Y \\ Z \end{bmatrix} = \begin{bmatrix} \cos \alpha \cos \beta & -\cos \alpha \sin \beta & -\sin \alpha \\ \sin \beta & \cos \beta & 0 \\ \sin \alpha \cos \beta & -\sin \alpha \sin \beta & \cos \alpha \end{bmatrix} \begin{bmatrix} -D \\ \bar{Y} \\ -\bar{L} \end{bmatrix} + \begin{bmatrix} T_{th} \\ 0 \\ 0 \end{bmatrix}$$

Proceeding in the same way for the aerodynamic moments can be obtained:

$$\begin{bmatrix} L \\ M \\ N \end{bmatrix} = \begin{bmatrix} \cos \alpha \cos \beta & -\cos \alpha \sin \beta & -\sin \alpha \\ \sin \beta & \cos \beta & 0 \\ \sin \alpha \cos \beta & -\sin \alpha \sin \beta & \cos \alpha \end{bmatrix} \begin{bmatrix} L' \\ M' \\ N' \end{bmatrix}$$

## 1.5 Compilation of Equations

In body frame:

$$\begin{bmatrix} X - mg \sin \theta \\ Y + mg \cos \theta \sin \phi \\ Z + mg \cos \theta \cos \phi \end{bmatrix} = m \begin{bmatrix} \dot{u} + qw - rv \\ \dot{v} + ru - pw \\ \dot{w} + pv - qu \end{bmatrix} + mL_{BE} \dot{W}_E$$

$$L = I_x \dot{p} - (I_y - I_z)qr$$

$$M = I_y \dot{q} - (I_z - I_x)rp$$

$$N = I_z \dot{r} - (I_x - I_y)pq$$

$$\begin{bmatrix} p \\ q \\ r \end{bmatrix} = \begin{bmatrix} \dot{\phi} - \dot{\psi} \sin \theta \\ \dot{\theta} \cos \phi + \dot{\psi} \cos \theta \sin \phi \\ -\dot{\theta} \sin \phi + \dot{\psi} \cos \theta \cos \phi \end{bmatrix}$$

$$\begin{bmatrix} \dot{\phi} \\ \dot{\theta} \\ \dot{\psi} \end{bmatrix} = \begin{bmatrix} p + (q \sin \phi + r \cos \phi) \tan \theta \\ q \cos \phi - r \sin \phi \\ (q \sin \phi + r \cos \phi) \sec \theta \end{bmatrix}$$

In the inertial frame:

$$\begin{aligned} m\ddot{x}_E &= X \cos \theta \cos \psi + Y(\sin \phi \sin \theta \cos \psi - \cos \phi \sin \psi) \\ &\quad + Z(\cos \phi \sin \theta \cos \psi + \sin \phi \sin \psi) \end{aligned}$$

$$m\ddot{y}_E = X \cos \theta \sin \psi + Y(\sin \phi \sin \theta \sin \psi + \cos \phi \cos \psi) \\ + Z(\cos \phi \sin \theta \sin \psi - \sin \phi \cos \psi)$$

$$m\ddot{z}_E = mg - X \sin \theta + Y \sin \phi \cos \theta + Z \cos \phi \cos \theta$$

$$L = I_y(\dot{\theta} \sin \phi - \dot{\psi} \cos \theta \cos \phi)(\dot{\theta} \cos \phi + \dot{\psi} \cos \theta \sin \phi) \\ + I_z(\dot{\theta} \cos \phi + \dot{\psi} \cos \theta \sin \phi)(-\dot{\theta} \sin \phi + \dot{\psi} \cos \theta \cos \phi) \\ + I_x(\ddot{\phi} - \ddot{\psi} \sin \theta - \dot{\psi} \dot{\theta} \cos \theta)$$

$$M = I_x(-\dot{\theta} \sin \phi + \dot{\psi} \cos \theta \cos \phi)(\dot{\phi} - \dot{\psi} \sin \theta) \\ + I_z(\dot{\psi} \sin \theta - \dot{\phi})(-\dot{\theta} \sin \phi + \dot{\psi} \cos \theta \cos \phi) \\ + I_y(\ddot{\theta} \cos \phi + \ddot{\psi} \cos \theta \sin \phi - \dot{\phi} \dot{\theta} \sin \phi \\ + \dot{\psi}(\dot{\phi} \cos \theta \cos \phi - \dot{\theta} \sin \theta \sin \phi))$$

$$N = I_x(-\dot{\theta} \cos \phi - \dot{\psi} \cos \theta \sin \phi)(\dot{\phi} - \dot{\psi} \sin \theta) \\ + I_y(\dot{\phi} - \dot{\psi} \sin \theta)(\dot{\theta} \cos \phi + \dot{\psi} \cos \theta \sin \phi) + I_z(-\dot{\theta} \sin \phi + \dot{\psi} \cos \theta \cos \phi \\ - \dot{\phi} \dot{\theta} \cos \phi - \dot{\psi}(\dot{\phi} \cos \theta \sin \phi + \dot{\theta} \sin \theta \cos \phi))$$

$$\begin{bmatrix} \dot{x}_E \\ \dot{y}_E \\ \dot{z}_E \end{bmatrix} \\ = \begin{bmatrix} \cos \theta \cos \psi & \sin \phi \sin \theta \cos \psi - \cos \phi \sin \psi & \cos \phi \sin \theta \cos \psi + \sin \phi \sin \psi \\ \cos \theta \sin \psi & \sin \phi \sin \theta \sin \psi + \cos \phi \cos \psi & \cos \phi \sin \theta \sin \psi - \sin \phi \cos \psi \\ -\sin \theta & \sin \phi \cos \theta & \cos \phi \cos \theta \end{bmatrix} \begin{bmatrix} u \\ v \\ w \end{bmatrix} \\ + \begin{bmatrix} W_{x_E} \\ W_{y_E} \\ W_{z_E} \end{bmatrix}$$

$$\begin{bmatrix} X \\ Y \\ Z \end{bmatrix} = \begin{bmatrix} \cos \alpha \cos \beta & -\cos \alpha \sin \beta & -\sin \alpha \\ \sin \beta & \cos \beta & 0 \\ \sin \alpha \cos \beta & -\sin \alpha \sin \beta & \cos \alpha \end{bmatrix} \begin{bmatrix} -D \\ \bar{Y} \\ -\bar{L} \end{bmatrix} + \begin{bmatrix} T_{th} \\ 0 \\ 0 \end{bmatrix}$$

$$\begin{bmatrix} L \\ M \\ N \end{bmatrix} = \begin{bmatrix} \cos \alpha \cos \beta & -\cos \alpha \sin \beta & -\sin \alpha \\ \sin \beta & \cos \beta & 0 \\ \sin \alpha \cos \beta & -\sin \alpha \sin \beta & \cos \alpha \end{bmatrix} \begin{bmatrix} L' \\ M' \\ N' \end{bmatrix}$$

$$D = \bar{q}SC_D \quad \bar{L} = \bar{q}SC_L \quad \bar{Y} = \bar{q}SC_Y$$

$$L' = \bar{q}SbC_l \quad M' = \bar{q}S\bar{c}C_m \quad N' = \bar{q}SbC_n$$

$$\bar{q} = \frac{1}{2}\rho V^2 \quad T_{th} = K_M \omega_M^2$$

## 1.6 Reduced Mathematical Model

The complete airplane model is separated into longitudinal and lateral-directional dynamics, assuming  $\beta \approx 0$  and  $\bar{Y} \approx 0$ , which leads to:

$$\left. \begin{aligned} X &= \bar{L} \sin \alpha + T_{th} - D \cos \alpha \\ Y &= \bar{Y} \\ Z &= -D \sin \alpha - \bar{L} \cos \alpha \end{aligned} \right\} (1.1) \quad \left. \begin{aligned} L &= L' \cos \alpha - N' \sin \alpha \\ M &= M' \\ N &= L' \sin \alpha + N' \cos \alpha \end{aligned} \right\} (1.2)$$

### Longitudinal model

For this dynamic, it is assumed that  $\phi \approx 0, \psi \approx 0$ , which reduces the equations of motion in the inertial frame to:

$$\left. \begin{aligned} m\dot{x}_E &= X \cos \theta + Z \sin \theta \\ m\dot{z}_E &= mg - X \sin \theta + Z \cos \theta \\ M &= I_y \ddot{\theta} \end{aligned} \right\} (1.3)$$

Now, equation (1.3) can be rewritten by substituting (1.1) and (1.2). Note that the term  $\frac{\tau_\theta}{I_y}$  comes from the assumption that the moment  $M$  is the moment given only by the geometry of the plane, so the moment  $\tau_\theta$  produced by the control surface is not included, and should be added as part of the total moment.

$$\left. \begin{aligned} \dot{x}_E &= \frac{\bar{L} \sin \alpha + T_{th} - D \cos \alpha}{m} \cos \theta - \frac{D \sin \alpha + \bar{L} \cos \alpha}{m} \sin \theta \\ \dot{z}_E &= g - \frac{\bar{L} \sin \alpha + T_{th} - D \cos \alpha}{m} \sin \theta - \frac{D \sin \alpha + \bar{L} \cos \alpha}{m} \cos \theta \\ \ddot{\theta} &= \frac{M}{I_y} + \frac{\tau_\theta}{I_y} \end{aligned} \right\} (1.4)$$

Defining the constants  $C_{0-4}$  with the correspondent constant coefficients:



$$C_0 = \frac{K_M}{m} \quad C_1 = -\frac{\rho S}{2m} C_D \quad C_2 = -\frac{\rho S}{2m} C_L \quad C_3 = \frac{\rho S \bar{c}}{2I_y} C_m \quad C_4 = \frac{1}{I_y}$$

Equation (1.4) is rewritten as

$$\left. \begin{aligned} \ddot{x}_E &= (C_1 \cos(\theta - \alpha) + C_2 \sin(\theta - \alpha))V^2 + \omega_M^2 C_0 \cos \theta \\ \ddot{z}_E &= g + (C_2 \cos(\theta - \alpha) - C_1 \sin(\theta - \alpha))V^2 - \omega_M^2 C_0 \sin \theta \\ \ddot{\theta} &= C_3 V^2 + C_4 \tau_\theta \end{aligned} \right\} (1.5)$$

### Lateral-directional model

The assumption made in this model is that :  $\theta \approx 0, \bar{Y} \approx 0$ , so the equations of motion in the inertial frame turn into:

$$\left. \begin{aligned} m\ddot{x}_E &= X \cos \psi + Z \sin \phi \sin \psi \\ m\ddot{y}_E &= X \sin \psi - Z \sin \phi \cos \psi \\ L &= I_x \ddot{\phi} \\ N &= I_z \ddot{\psi} \end{aligned} \right\} (1.6)$$

Then, equation (1.6) can be rewritten by substituting (1.1) and (1.2). Note that as in equation (1.4), the moments  $L$  and  $N$  correspond to the plane geometry, so the terms  $\frac{\tau_\phi}{I_x}$  and  $\frac{\tau_\psi}{I_z}$  that come from the moments  $\tau_\phi$  and  $\tau_\psi$  produced by the control surfaces, are added, leading to.

$$\left. \begin{aligned} \ddot{x}_E &= \frac{\bar{L} \sin \alpha + T_{th} - D \cos \alpha}{m} \cos \psi - \frac{D \sin \alpha + \bar{L} \cos \alpha}{m} \sin \phi \sin \psi \\ \ddot{y}_E &= \frac{\bar{L} \sin \alpha + T_{th} - D \cos \alpha}{m} \sin \psi + \frac{D \sin \alpha + \bar{L} \cos \alpha}{m} \sin \phi \cos \psi \\ \ddot{\phi} &= \frac{L' \cos \alpha - N' \sin \alpha}{I_x} + \frac{\tau_\phi}{I_x} \\ \ddot{\psi} &= \frac{L' \sin \alpha + N' \cos \alpha}{I_z} + \frac{\tau_\psi}{I_z} \end{aligned} \right\} (1.7)$$

Defining the constants  $C_{5-10}$  with the correspondent constant coefficients, (1.7) is rewritten:

$$C_5 = \frac{\rho S b}{2I_z} C_l \quad C_6 = \frac{\rho S b}{2I_z} C_n \quad C_7 = \frac{1}{I_z} \quad C_8 = \frac{\rho S b}{2I_x} C_l \quad C_9 = \frac{\rho S b}{2I_x} C_n \quad C_{10} = \frac{1}{I_x}$$

$$\begin{aligned} \ddot{x}_E = & (C_1(\cos \alpha \cos \psi + \sin \alpha \sin \emptyset \sin \psi) + C_2(\cos \alpha \sin \emptyset \sin \psi - \sin \alpha \cos \psi))V^2 \\ & + C_0\omega_M^2 \cos \psi \end{aligned}$$

$$\begin{aligned} \ddot{y}_E = & (C_1(\cos \alpha \sin \psi - \sin \alpha \sin \emptyset \cos \psi) - C_2(\sin \alpha \sin \psi + \cos \alpha \sin \emptyset \cos \psi))V^2 \\ & + C_0\omega_M^2 \sin \psi \end{aligned}$$

$$\ddot{\emptyset} = (C_8 \cos \alpha - C_9 \sin \alpha)V^2 + C_{10}\tau_\emptyset$$

$$\ddot{\psi} = (C_5 \sin \alpha + C_6 \cos \alpha)V^2 + C_7\tau_\psi$$

Considering  $\alpha = 0$

$$\left. \begin{aligned} \ddot{x}_E &= (C_1 \cos \psi + C_2 \sin \emptyset \sin \psi)V^2 + C_0\omega_M^2 \cos \psi \\ \ddot{y}_E &= (C_1 \sin \psi - C_2 \sin \emptyset \cos \psi)V^2 + C_0\omega_M^2 \sin \psi \\ \ddot{\emptyset} &= C_8 V^2 + C_{10}\tau_\emptyset \\ \ddot{\psi} &= C_6 V^2 + C_7\tau_\psi \end{aligned} \right\} \quad (1.8)$$

## 1.7 Trajectory Parameterization

The first remark that needs to be done is the difference between path following and reference tracking. In path following, the system is forced to follow a geometric path without constraints in time, while in reference tracking, the system has to follow a reference signal dependent on time, for that reason, path following is thought more flexible.

In the case where path following is used to follow a trajectory, as said above, the geometric path needs to be time-independent, this fact force us to make the trajectory time-independent, in other words, the trajectory needs to be reparametrized.

The reparametrization done in this work is by the arclength, in this way, the “checkpoints” of the path that will be followed, are controlled.

In order to begin with the trajectory reparametrization, some background on this subject is presented.

A vector function  $f: (a, b) \rightarrow \mathbb{R}^3$  is class  $C^k$  ( $k = 0, 1, 2, \dots$ ) if  $f$  and its first derivatives,  $f', f'', \dots, f^k$ , exist and are all continuous. The function  $f$  is *smooth* if  $f$  is  $C^k$  for every positive integer  $k$ . A *parametrized curve* is a  $C^3$  (or smooth) map  $\alpha: I \rightarrow \mathbb{R}^3$  for some interval  $I = (a, b)$  or  $[a, b]$  in  $\mathbb{R}$  (possibly infinite). We say  $\alpha$  is regular if  $\alpha'(t) \neq 0$  for all  $t \in I$ , where  $t$  receives the name of *parameter* of the curve.

If  $\alpha: [a, b] \rightarrow \mathbb{R}^3$  is a parametrized curve, then for any  $a \leq t \leq b$ , it is defined its *arclength* from  $a$  to  $t$  to be  $s(t) = \int_a^t \|\alpha'(u)\| du$ . That is, the distance a particle travels the arclength of its trajectory is the integral of its speed.

Let  $\alpha: [a, b] \rightarrow \mathbb{R}^3$  be a continuous parametrized curve. Given a partition  $\mathcal{P} = \{a = t_0 < t_1 \dots < t_k = b\}$  of the interval  $[a, b]$ , let

$$\ell(\alpha, \mathcal{P}) = \sum_{i=1}^k \|\alpha(t_i) - \alpha(t_{i-1})\|$$

That is,  $\ell(\alpha, \mathcal{P})$  is the length of the inscribed polygon with vertices at  $(t_i)$ ,  $i = 0, \dots, k$ , as indicated in Fig. 1.5. The arclength of  $\alpha$  is defined as

$$\ell(\alpha) = \sup \{\ell(\alpha, \mathcal{P}) | \mathcal{P} \in \text{Partition of } [a, b]\}$$

where *sup* stands for the supreme.

A curve is said to be *rectifiable* if has a finite arclength.

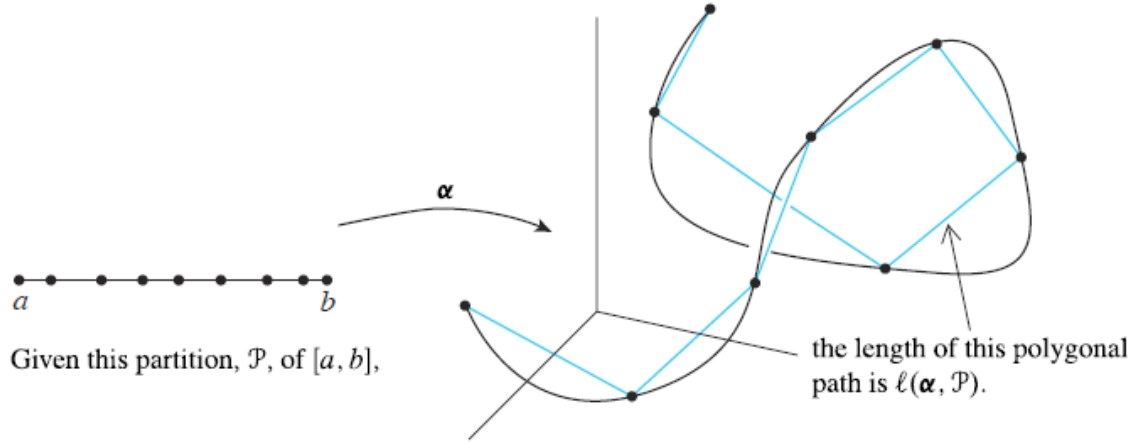


Fig. 1.4: Arclength definition.

Definition. Let  $\alpha: [a, b] \rightarrow \mathbb{R}^3$  be a piecewise  $C^1$  parametrized curve. Then the arclength can be denoted as

$$\ell(\alpha) = \int_a^b \|\alpha'(t)\| dt \quad (1.9)$$

Now, for  $a \leq t \leq b$ , define  $s(t)$  to be the length of the curve  $\alpha$  on the interval  $[a, t]$ , then, the curve  $\alpha$  is *parametrized by arclength* if  $s(t) = t$  for all  $t$ . In this event, it is likely to use the parameter  $s \in [0, L]$  and write  $\alpha(s)$ .

## 1.8 Serret-Frenet frame.

What distinguish a circle or a helix from a line is their *curvature*, i.e., the tendency of the curve to change direction. In this section, it is seen how can be associated to each smooth ( $C^3$ ) arclength-parametrized curve  $\alpha$  a natural moving frame (an orthonormal basis for  $\mathbb{R}^3$  chosen at each point on the curve, adapted to the geometry of the curve as much as possible), called the Serret-Frenet frame.

The term  $\alpha'(s) = \frac{\partial \alpha(s)}{\partial s}$  is the *unit tangent vector* to the curve, denoted by

$$\vec{t}(s) = \frac{\alpha'(s)}{\|\alpha'(s)\|}$$

Since  $\vec{t}(s)$  has constant length,  $\vec{t}'(s) = \frac{\partial \vec{t}(s)}{\partial s}$  will be orthogonal to  $\vec{t}(s)$ . Assuming  $\vec{t}'(s) \neq 0$ , it is defined the *principal normal vector*.

$$\vec{n}(s) = \frac{\vec{t}'(s)}{\|\vec{t}'(s)\|} = \frac{\alpha''(s)}{\|\alpha''(s)\|}$$

The curvature, expressed by  $\kappa(s) = \frac{\|\alpha'(s) \times \alpha''(s)\|}{\|\alpha'(s)\|^3}$ , leads to

$$\frac{\partial \vec{t}(s)}{\partial s} = \kappa(s) \vec{n}(s) \quad (1.10)$$

Moreover, assuming that  $\kappa(s) \neq 0$ , the *binomial vector* is defined as

$$\vec{b}(s) = \vec{t}(s) \times \vec{n}(s)$$

Then, the right-handed orthonormal basis for  $\mathbb{R}^3$  attached to the moving particle will be denoted by  $F_F\{\vec{t}(s), \vec{n}(s), \vec{b}(s)\}$ . Note that  $\vec{n}'(s)$  must be a linear combination of  $\vec{t}(s)$ ,  $\vec{n}(s)$ , and  $\vec{b}(s)$  and it is known that  $\vec{n}'(s) \cdot \vec{n}(s) = 0$  and  $\vec{n}'(s) \cdot \vec{t}(s) = -\vec{t}'(s) \cdot \vec{n}(s) = -\kappa(s)$ , therefore, defining the *torsion*  $\tau(s) = \vec{n}'(s) \cdot \vec{b}(s)$ , it is obtained

$$\frac{\partial \vec{n}(s)}{\partial s} = -\kappa(s) \vec{t}(s) + \tau(s) \vec{b}(s) \quad (1.11)$$

Finally,  $\vec{b}'(s)$  must be a linear combination of  $\vec{t}(s)$ ,  $\vec{n}(s)$ , and  $\vec{b}(s)$  and it is known that  $\vec{b}'(s) \cdot \vec{b}(s) = 0$ ,  $\vec{b}'(s) \cdot \vec{t}(s) = -\vec{t}'(s) \cdot \vec{b}(s) = 0$ , and  $\vec{b}'(s) \cdot \vec{n}(s) = -\vec{n}'(s) \cdot \vec{b}(s) = -\tau(s)$ , leading to

$$\frac{\partial \vec{b}(s)}{\partial s} = -\tau(s) \vec{n}(s) \quad (1.12)$$

Being equations (1.10)-(1.12) the Serret-Frenet formulas where the curvature is always nonnegative. For more information please refer to [3].

To let this point clear, here is shown an example with a circular trajectory.

A circle can be parameterized by an angle  $\theta$  (see Fig. 1.5):

$$\alpha(\theta) = (r \cos \theta, r \sin \theta)$$

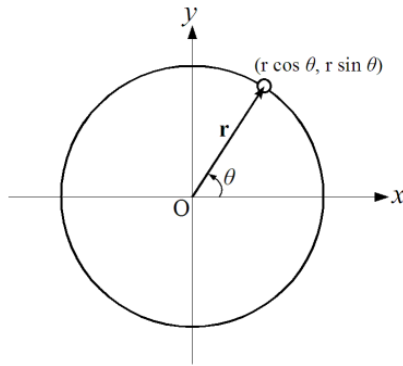


Fig. 1.5: Circular trajectory parameterized by  $\theta$ .

Then, obtaining the derivative with respect to  $\theta$ , it is obtained:

$$\alpha'(\theta) = (-r \sin \theta, r \cos \theta)$$

$$\|\alpha'(\theta)\| = \sqrt{r^2(\sin^2 \theta + \cos^2 \theta)} = r$$

Using the equation (1.9):

$$l(\alpha) = \int_{\theta_0}^{\theta} r d\theta = r\theta$$

And searching for the reparametrization

$$g(l(\alpha)) = r\theta$$

Obtaining the derivative with respect to  $\theta$

$$g'(l(\alpha))l'(\alpha) = r$$

Then, it is know that  $l'(\alpha) = \|\alpha'(\theta)\| = r$ , so

$$g'(l(\alpha)) = 1$$

Integrating using the new parameter  $s$ :

$$g(l(\alpha)) = r\theta = \int_0^s (1) ds = s$$

Leading to:  $\theta = \frac{s}{r}$

Once this relation is obtained, the curve can be reparametrized as

$$\alpha(s) = \left( r \cos \frac{s}{r}, r \sin \frac{s}{r} \right)$$

Probing this equation using Matlab code, it was obtained the Fig. 1.6

```
r=1;  
s=.1:.1:2*pi;  
plot(r*cos(s/r),r*sin(s/r))
```

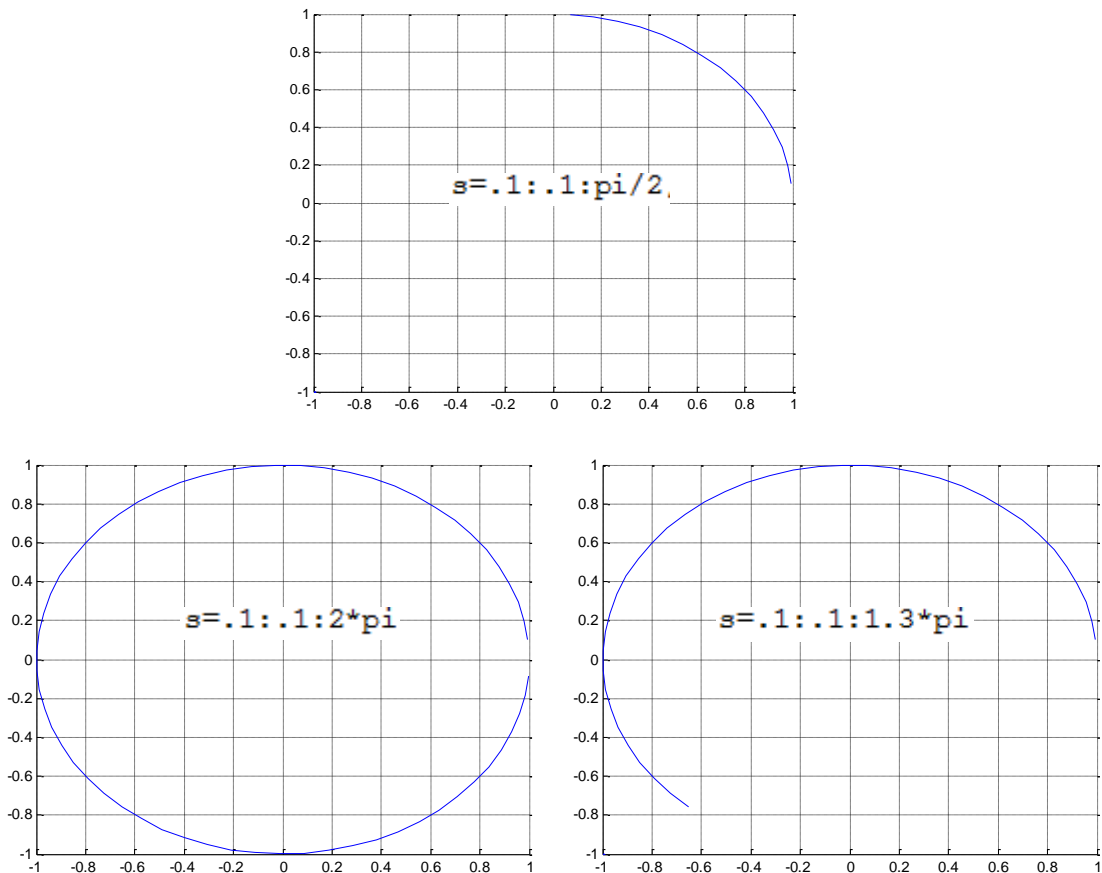


Fig. 1.6: Circular trajectory parameterized by arc length.

Then, obtaining the frame attached to the virtual particle moving along the trajectory, i.e., the Serret-Frenet frame, it is first obtained that:

$$\alpha'(s) = \left( -\sin \frac{s}{r}, \cos \frac{s}{r}, 0 \right) \quad \|\alpha'(s)\| = 1$$

$$\alpha''(s) = \left( -\frac{1}{r} \cos \frac{s}{r}, -\frac{1}{r} \sin \frac{s}{r}, 0 \right) \quad \|\alpha''(s)\| = \frac{1}{r}$$

Then, according to equations (1.10)-(1.12), the Serret-Frenet frame will be denoted by.

$$\vec{t}(s) = \frac{\alpha'(s)}{\|\alpha'(s)\|} = \left( -\sin \frac{s}{r}, \cos \frac{s}{r}, 0 \right)$$

$$\vec{n}(s) = \frac{\alpha''(s)}{\|\alpha''(s)\|} = \left( -\cos \frac{s}{r}, -\sin \frac{s}{r}, 0 \right)$$

$$\vec{b}(s) = \vec{t}(s) \times \vec{n}(s) = (0, 0, 1)$$

Finally, the curvature of a circular path will be given by:

$$\kappa(s) = \frac{1}{r}$$

As the trajectory is expressed in two dimensions the torsion is not considered.



## **Chapter 2.**

### **Path following**

Several military and civilian applications on path following and trajectory tracking have already been studied and diversified for UAV's during the last years, so the second part of this work refers to the problem statement of path following and trajectory tracking as well as one approach for each.

In general, the problem statement is that given a desired trajectory and knowing the position of the vehicle as well as its heading angle, the necessary heading angle to follow this trajectory should be found. The angle denoted by the tangent line in certain point of the trajectory and the inertial frame is called Line-of-Sight (LOS), and the distance existent between the vehicle and certain point in the trajectory is called cross-track error. The main idea of the path following is to minimize the cross-track error and make the vehicle heading angle converge to the LOS angle.

For now, trajectory it's considered only in two dimensions, altitude will be neglected and taken as a constant.

#### **2.1 First approach**

The first goal of this work was to have a functional experimental platform equipped with the necessary sensors to be able to follow a trajectory, that is why the first approach taken needed to be easy to implement and enough accurate, moreover, the circle was chosen as a desired trajectory, the reason is that every trajectory can be described in circles of varying radius, even straight lines (circles with a very long radius). The approach is described as follows and is the first implementation on the experimental platform, inspired in [4].

This method, besides being simple and easy to apply, it is shown to have a benefit over linear approaches for curved paths. It contains an element of anticipation for the upcoming local desired flight path.

The guidance logic selects a reference point on the desired trajectory and generates a lateral acceleration command using the reference point. The reference point is on the desired path at a distance  $L_1$  forward of the vehicle. The angle created from  $V$  (the vehicle velocity) to the line  $L_1$  (clockwise direction is positive) is defined as  $\eta$ . Moreover,  $d$  stands for the cross-track error,  $R$  for the radius of circle or circular segment and  $a_{scmd}$  for the acceleration command sideways i.e. perpendicular to vehicle velocity direction.

At each time-step, a circular path (tangent to the vehicle velocity vector) can be defined by the position of the reference point and the vehicle position, as shown in Fig. 2.1 by the dotted line.

The acceleration command is equal to the centripetal acceleration required to follow this circular arc, expressing this fact in equations, a sinus law is needed:

$$\frac{L_1}{\sin 2\eta} = \frac{R}{\sin(90 - \eta)}$$

$$\sin 2\eta = 2\sin \eta \cos \eta \qquad \sin(90 - \eta) = \cos \eta$$

$$\frac{L_1}{2\sin \eta \cos \eta} = \frac{R}{\cos \eta}$$

$$L_1 = 2R \sin \eta \quad \rightarrow \quad \frac{1}{R} = \frac{2 \sin \eta}{L_1} \qquad (2.1)$$

From centripetal acceleration in uniform circular motion, and using equation (2.1):

$$a_{scmd} = \frac{V^2}{R} = 2 \frac{V^2 \sin \eta}{L_1}$$

$$a_{scmd} = 2 \frac{V^2}{L_1} \sin \eta \quad (2.2)$$

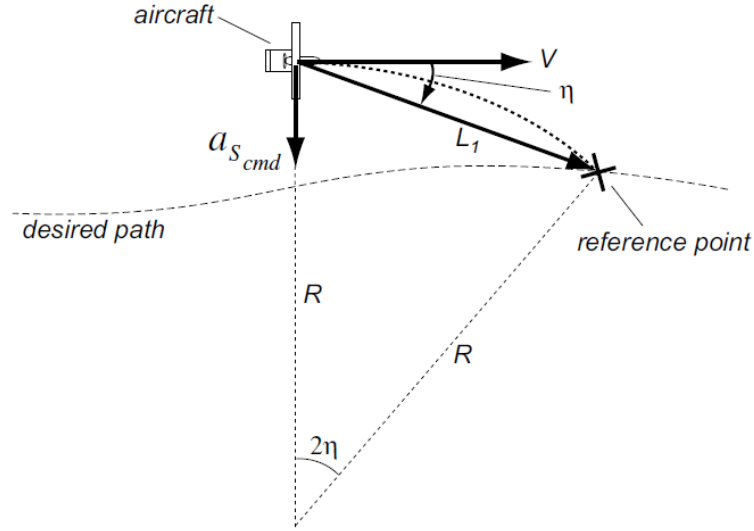


Fig. 2.1: Diagram for Guidance Logic.

The direction of the acceleration depends on the sign of the angle between the  $L_1$  line segment and the vehicle velocity vector, consequently, when the selected reference point is to the right of the vehicle velocity vector, the vehicle will be commanded to accelerate to the right, and viceversa for position to left.

Hence, the guidance logic will produce a lateral acceleration expressed by equation (2.2) that is appropriate to follow a circle of any radius  $R$ . This lateral acceleration will cause that the velocity direction of the plane rotates until the velocity direction is aligned with the direction of the  $L_1$  segment, this can be showed by:

$$\omega = \frac{V}{R}$$

Which is the angular velocity equation for a uniform circular motion.

From the centripetal acceleration:

$$a_{scmd} = \frac{V^2}{R} = \omega V \rightarrow \omega = \frac{a_{scmd}}{V} \quad (2.3)$$

Using the angular velocity definition in a time-step increment:

$$\omega = \frac{\Delta\psi}{\Delta t} \rightarrow \Delta\psi = \omega\Delta t$$

Then, using (2.3) it leads to:

$$\Delta\psi = \frac{a_{scmd}}{V} \Delta t$$

Equation that shows the change in orientation, therefore, a change in velocity direction due to the acceleration.

It is worth to note that when the direction of  $L_1$  makes a larger angle with the desired path, is when the vehicle is far away from the desired path, and when the vehicle is close to the desired path, the angle is small. Therefore, if the vehicle is far away the desired path, the guidance logic tends to rotate the vehicle so that its velocity direction approaches the desired path at a large angle. On the other hand, if the vehicle is close to the desired path, the guidance logic rotates the vehicle so that its velocity direction approaches the desired path at a small angle.

### Following a Circular Path

The Fig. 2.2 shows the angles and distances that are taken into account, the angles  $\eta_1$  and  $\eta_2$  are considered small, but  $\eta_3$  not necessarily, also, is considered that

$$\eta = \eta_1 + \eta_2 + \eta_3.$$

The angle  $\eta_3$  is associated with the local circular segment, the current position of the vehicle is denoted by  $r = R + d$ . The angle  $\psi$  indicate the velocity direction.

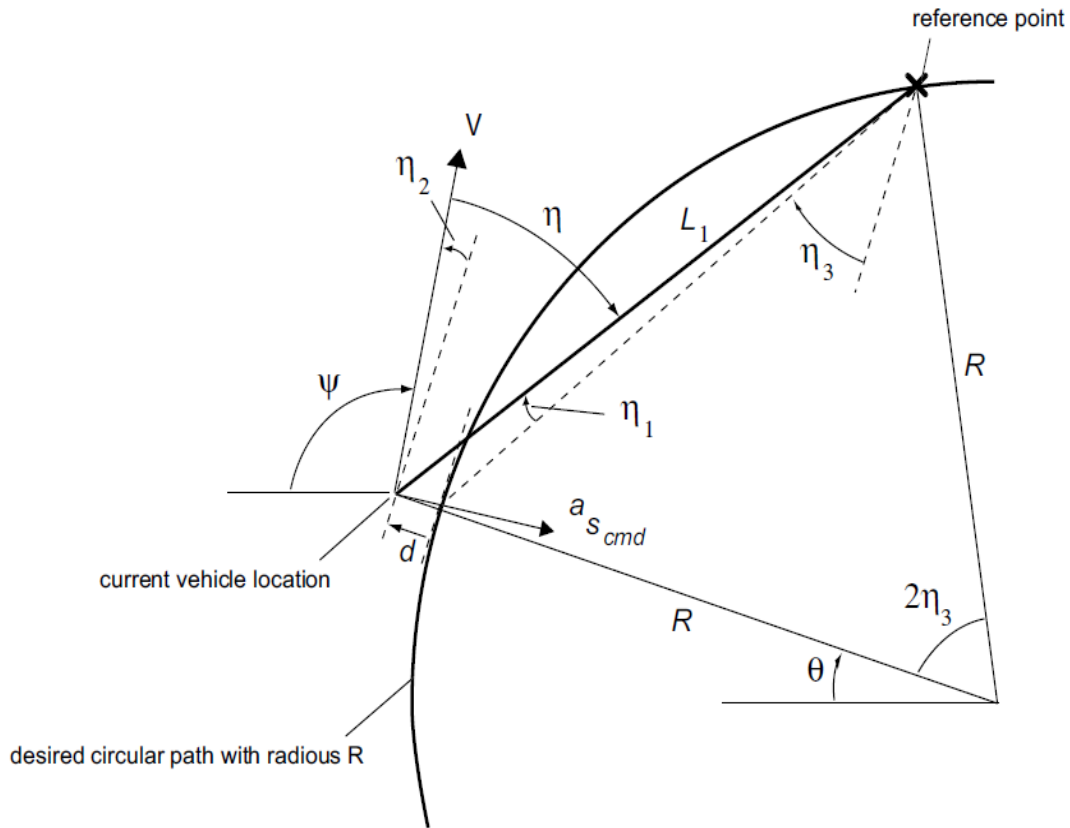


Fig. 2.2: Circular path following.

The angle  $\eta_2$  is an angle created by the difference between the velocity direction and the current tangent line to the circular desired path, the relation of these three angles is:

$$\psi - \theta + \eta_2 = \frac{\pi}{2}$$

Obtaining the derivative:

$$\dot{\psi} = \dot{\theta} - \dot{\eta}_2 \quad (2.4)$$

Then, recalling the assumption of  $\eta_1 + \eta_2 + \eta_3$ , but considering  $\eta_1 \approx 0$  and  $\eta_2 \approx 0$  and using equation (2.1), it is obtained:

$$\frac{L_1}{2R} \approx \sin \eta_3$$

Consequently, from trigonometry

$$\sin^2 \eta_3 + \cos^2 \eta_3 = 1 \quad (2.5)$$

And obtaining the term  $\cos \eta_3$  from equation (2.5)

$$c \equiv \cos \eta_3 \approx \sqrt{1 - \left(\frac{L_1}{2R}\right)^2}$$

Then, from the angle assumption that  $\eta_2 \approx 0$ , the rate of change of the cross track error is

$$\dot{d} = V \sin \eta_2 \approx V \eta_2$$

And its derivative, assuming that  $V$  is constant.

$$\ddot{d} = V \dot{\eta}_2 \quad (2.6)$$

Then, using equations (2.3), (2.4) and (2.6), under the assumption  $\dot{\psi} = \dot{\theta}$ , the lateral acceleration can be expressed as:

$$a_{scmd} = V \dot{\psi} = V \dot{\theta} - V \dot{\eta}_2 = V \dot{\theta} - \ddot{d} \quad (2.7)$$

Assuming small angles on  $\eta_1$  and  $\eta_2$ , equation (2.7) can be rewritten as:

$$V \dot{\theta} = \frac{V^2}{R}$$

Which leads to the equation of the centripetal acceleration to follow the circle with radius  $R$  at speed  $V$ . Then

$$a_{scmd} = \frac{V^2}{R} - \ddot{d} \quad (2.8)$$

Developing equation (2.2) with the considerations of  $\eta_1 \approx 0$  and  $\eta_2 \approx 0$

$$2 \frac{V^2}{L_1} \sin \eta = 2 \frac{V^2}{L_1} \sin(\eta_1 + \eta_2 + \eta_3)$$

Using the property  $\sin(x + y) = \sin x \cos y + \cos x \sin y$

It leads to:

$$\begin{aligned}
 2 \frac{V^2}{L_1} \sin \eta &= 2 \frac{V^2}{L_1} \{ \sin(\eta_1 + \eta_2) \cos \eta_3 + \cos(\eta_1 + \eta_2) \sin \eta_3 \} \\
 2 \frac{V^2}{L_1} \sin \eta &= 2 \frac{V^2}{L_1} \{ (\eta_1 + \eta_2) \cos \eta_3 + \sin \eta_3 \} \\
 2 \frac{V^2}{L_1} \sin \eta &= 2 \frac{V^2}{L_1} \{ \eta_1 \cos \eta_3 + \eta_2 \cos \eta_3 + \sin \eta_3 \} \quad (2.9)
 \end{aligned}$$

Substituting relations:

$$\eta_1 \approx \frac{d}{L_1} \cos \eta_3 \quad \eta_2 \approx \frac{\dot{d}}{V} \quad c \equiv \cos \eta_3 \approx \sqrt{1 - \left(\frac{L_1}{2R}\right)^2} \quad \frac{L_1}{2R} \approx \sin \eta_3$$

Equation (2.9) is rewritten as

$$\begin{aligned}
 2 \frac{V^2}{L_1} \sin \eta &= 2 \frac{V^2}{L_1} \left\{ \frac{d}{L_1} c^2 + \frac{\dot{d}}{V} c + \frac{L_1}{2R} \right\} = 2 \frac{V^2 c^2}{L_1^2} d + 2 \frac{Vc}{L_1} \dot{d} + \frac{V^2}{R} \\
 2 \frac{V^2}{L_1} \sin \eta &= 2 \frac{V^2 c^2}{L_1^2} d + 2 \frac{Vc}{L_1} \dot{d} + \frac{V^2}{R} \quad (2.10)
 \end{aligned}$$

Finally, substituting (2.8) and (2.10) into (2.2), yields to:

$$\ddot{d} + 2 \frac{Vc}{L_1} \dot{d} + 2 \frac{V^2 c^2}{L_1^2} d \approx 0 \quad (2.11)$$

This means that the centripetal acceleration needed to follow the desired path is the same as the acceleration command sideways given to the plane.

Consequently, equation (2.11) can be expressed by the following linear second order characteristic equation.

$$\ddot{d} + 2\xi\omega_n\dot{d} + \omega_n^2 d \approx 0$$

The fact that this equation is the same as the linear second order equation with zero-input, it allows to assure that if the values of the damping factor  $\xi$  and the natural frequency  $\omega_n$  are under specific circumstances, the variable  $d \rightarrow 0$  as  $t \rightarrow \infty$ .

In this case, the damping factor  $\xi = \frac{1}{\sqrt{2}} = .7071$  and natural frequency  $\omega_n = \sqrt{2} \frac{Vc}{L_1}$ , belong to an underdamped case (as  $0 < \xi < 1$ ), therefore, when the distance  $L_1$  is chosen wisely, the crosstrack error  $d \rightarrow 0$  as  $t \rightarrow \infty$ .

For more information please refer to [4].



## 2.2 Second approach

There exist several methods of path following using different control strategies, which were compared in a survey of unmanned aerial vehicles [5] made in 2014, where the performance was evaluated with the total control effort (quantification of the algorithm's control demand) and the total cross-tracking error (vehicle's offset with respect to the desired trajectory).

Among the algorithms considered, the carrot-chasing algorithm, which is easy to implement, with respect to algorithms such as VF (Vector Field), PLOS (Pure Line of Sight), NLGL (Non Linear Guidance Law) and LQR (Linear Quadratic Regulator) showed to have had the worst performance due to the lack of robustness under wind disturbances, which leads to an opportunity to improve the weak points on this algorithm.

The carrot chasing algorithm consists on introducing a virtual target (imaginary particle) in the desired trajectory and make the vehicle to chase this target [18]; In this work, the virtual target will follow a trajectory denoted by the equation obtained from the reparametrization of a circle.

The VF (Vector Field) method calculates a vector field around the path to be tracked, where the vectors are directed toward the path and serve as course commands to the plane. The PLOS (Pure Line of Sight) is a combination of Pure pursuit and Line-Of-Sight guidance law, where the Pure pursuit drives the UAV to a waypoint, while the LOS guidance law steers the vehicle toward the LOS. The LQR (Linear Quadratic Regulator) is a method where the control effort is computed using optimal control theory in order to minimize the cross-track error. The NLGL (Non Linear Guidance Law) uses also a virtual target concept.

Based on the Dubins Aircraft, term introduced in [6], which extends the Dubins Car model [7] to an airplane and which is a reduction of the lateral dynamics of the complete airplane model, previously used in other works such as [8][9], the model

that will be used in this work, can be extracted from the Fig. 2.3, where it can be seen how the groundspeed  $V_E$  involves the relative velocity of the plane (airspeed  $V$ ) and also the wind velocity  $W$ , furthermore, despite of the fact that the plane holds a yaw angle  $\psi$ , when a wind gust is present, the flight path angle  $\psi_g$  may not be the same, as is affected by the wind direction, denoted by the angle  $\psi_w$ , under this assumptions, the following equations are obtained:

$$\left. \begin{aligned} x_E &= V \cos \psi + W \cos \psi_w \\ y_E &= V \sin \psi + W \sin \psi_w \\ \dot{\psi} &= \omega \end{aligned} \right\} \quad (2.12)$$

## 2.2.1 Introduction to Wind Estimation

There are several approaches to manage wind disturbances, a wind model can be developed, unfortunately, many factors such as air pressure, height, moisture, terrain, temperature, and so on, can affect the instability and randomness of the wind field, so it's difficult to build the exact mathematical model. As another method, a wind field estimation comparing measures of aircraft motion with respect to predictions of the dynamical model can be done, and despite of the fact that it is simple and in real time, it has as a drawback the need of certain navigation equipments and the lack of good precision as it relies on noisy measurements with errors depending on each sensor.

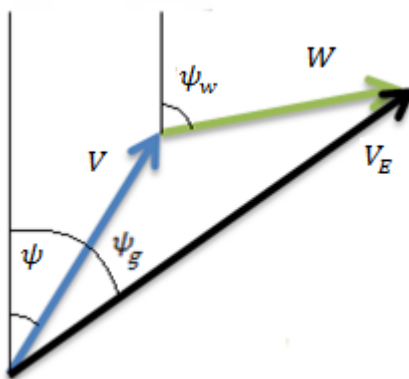


Fig. 2.3: Wind triangle.

Regarding to the wind management, which is very important for navigation purposes, and knowing that the plane in this work moves with a low airspeed, comparable with the wind gusts, a research of wind estimation is presented.

It is seen in [10], how the wind magnitude, direction and a scaling factor (factor who gives de proper relation to convert the dynamic pressure measured in the Pitot's tube into airspeed) are estimated using an Extended Kalman Filter, where the evolution model of these variables is represented as a random walk process and the nonlinearity is only in the observation model, however, the wind parameters are considered constants under the assumption that the wind shear (change in direction and/or velocity of the wind field between two points within the atmosphere) doesn't change in a radius of 32 kilometers, this approach was validated in a 2.5m wingspan airplane and using an Automatic Weather Station with a wind profile power-law to obtain the wind velocity at certain altitude based on the wind velocity at a reference low altitude.

$$u_z = u_r \left( \frac{z}{z_r} \right)^p$$

$u_z$  = Wind velocity at  $z$  altitude

$u_r$  = Wind velocity at  $z_r$  reference altitude

$p$  = Power law exponent proposed

In [11], an estimation of the attitude is improved using the fusion of GPS/INS measures and wind estimation (3 component wind velocity vector as well as the sideslip and attack angles) via an UKF (Unscented Kalman Filter) rather than only using the GPS/INS measures, sideslip and attack angle are measured with small wind vanes attached to potentiometers. The wind dynamic is given as a random walk process.

In [12], the 3 component wind velocity vector is estimated as a disturbance using a Nonlinear disturbance observer in order to improve a Dubins-based path following

algorithm, also validated in practice with a small airplane. In this approach, the wind dynamic is considered nearly zero, it means,  $\dot{W}_E \approx 0$ .

In [13], not only wind velocity is estimated, but also the net rate of change of the wind velocity, these are computed from vehicle response, the method relies in comparing measurements of airplane motion given by inertial sensor and gps, and predictions of dynamic model (separated into two parts, motion induced by the state and control inputs and motion induced by the wind field), moreover, simulations of wind gusts are done to validate the method using the Dryden's mathematical wind model, approach preferred for the US Department of Defense in 1990.

It is worth to say that Dryden's and Von Kármán wind models are the most common continuous wind gust models for flight dynamics applications. These two models, based on the military report *MIL-F-8785* or in the military handbook *MIL-HDBK-1797* are considered as:

- Stationary Gaussian Process: Stochastic process whose probability distribution besides being Gaussian, does not change in time.
- Homogeneous: The model can be applied in any space, it means, it not depends on the vehicle trajectory.
- Ergodic: Model has the same behavior averaged over time as averaged over the space, implying that the system has repeatability.
- Uniform in all orientations at high altitudes.

In [14], dynamic soaring is achieved estimating wind with a Kalman filter, assuming a polynomial representation dependent on altitude of wind fields.

In [15], using the lateral dynamic of a plane, an estimation of a constant wind field via an adaptive backstepping method is proposed. In [16], a wind computation based on the vehicle response was simulated; besides, a wind estimation using the latter adaptive backstepping method was proposed to make on-line wind estimation, synthesizing the equations into a minimum-order design with tuning functions.

In [17], using ground referenced measurements instead of the plane measurements, in conjunction with the vector field approach to control a path following task, wind-disturbance is shown to be rejected significantly.

## 2.2.2 Path following Model

In this section, the cross-track error (distance  $d$  between the point  $p$  and  $q$ ) and LOS error (angle between the airspeed vector and the tangent to the path at the point  $q$ ), see Fig. 2.4, are modeled using as a reference the work made by Micaelli and Samson(1993) [18], work which is still used as in [12].

The airplane center of mass position in two dimensions in the inertial frame is given by the coordinates  $p = [x_E \ y_E]^T$ , and the position of the imaginary target in the inertial frame as  $q(s) = [s_x \ s_y]^T$ , moreover, the airspeed is denoted by  $V$ , heading angle as  $\psi$ , and a turning rate around yaw is denoted by  $\omega$ , the inertial vector error  $d_I$  is defined and decomposed in the Serret-Frenet frame as  $d_F = [e_x \ e_y]^T$ , and the assumption that the airplane flights at a desired constant altitude  $h^d$  is made.

To compute the heading angle in the Serret-Frenet frame, the geometry of the path can be exploited. It must be recalled from Section 1.8 the desired path parametrized by arclength  $\alpha(s)$ , where its derivative  $\alpha'(s)$  is the tangent vector to the path, so that:

$$\psi_f = \tan^{-1} \frac{S_y'}{S_x'}$$

Rotational matrix between inertial and Serret Frenet frame can be denoted as:

$$R^{IF}(\psi_f) = \begin{bmatrix} \cos \psi_f & -\sin \psi_f \\ \sin \psi_f & \cos \psi_f \end{bmatrix} \quad R^{FI}(\psi_f) = \begin{bmatrix} \cos \psi_f & \sin \psi_f \\ -\sin \psi_f & \cos \psi_f \end{bmatrix}$$

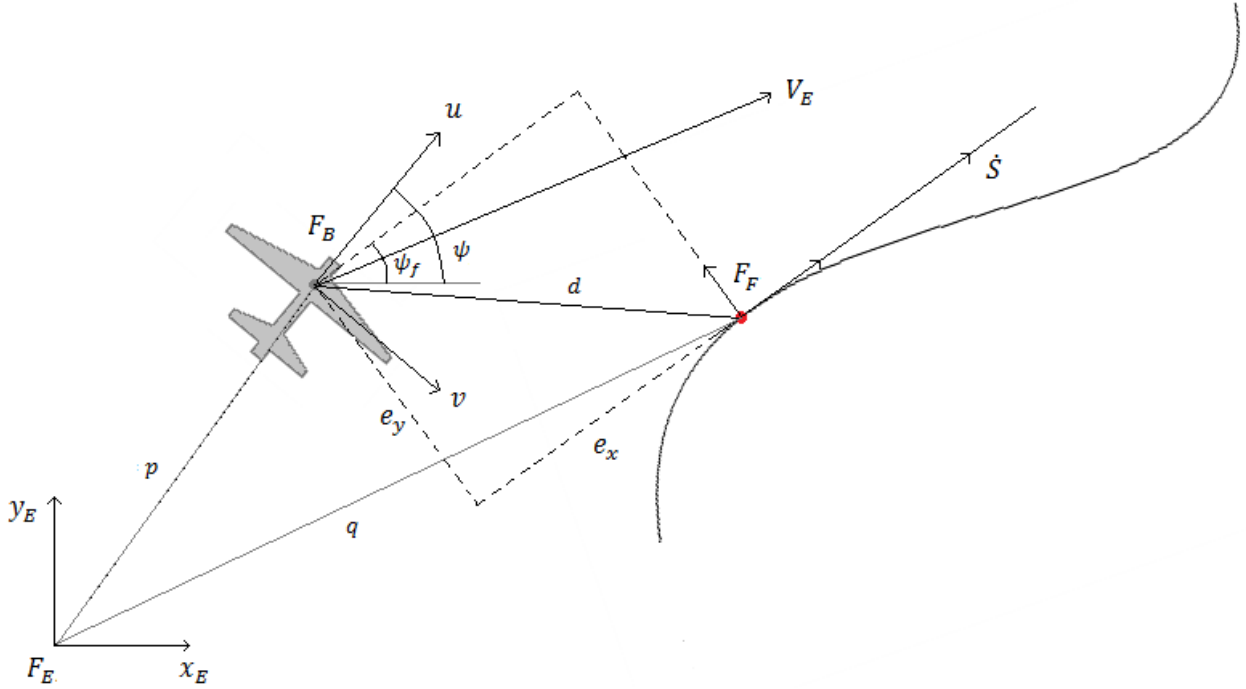


Fig. 2.4: Path Following figure.

Then, the cross-track error (vector error) and its derivative in the Serret-Frenet frame will be:

$$d_F = \begin{bmatrix} e_x \\ e_y \end{bmatrix} = R^{FI}(\psi_f)d_I = R^{FI}(\psi_f)(p - q(s))$$

$$\dot{d}_F = R^{FI}(\psi_f)\dot{d}_I + \dot{R}^{FI}(\psi_f)d_I \quad (2.13)$$

Where the inertial vector error is denoted by

$$d_I = p - q(s)$$

And its derivative

$$\dot{d}_I = \dot{p} - \dot{q}(s)$$

Then (2.13) is rewritten:

$$\dot{d}_F = R^{FI}(\psi_f)(\dot{p} - \dot{q}(s)) + \dot{R}^{FI}(\psi_f)(p - q(s)) \quad (2.14)$$

Without forgetting the Euler's property

$$R^{FI}(\psi_f) = -GR^{FI}$$

Where  $G$  is the skew symmetric matrix of the angular velocity, and, equally, knowing that  $G^T = -G$ , then:

$$G = \begin{bmatrix} 0 & -\dot{\psi}_f \\ \dot{\psi}_f & 0 \end{bmatrix}$$

Therefore, equation (2.14) turns into:

$$\dot{d}_F = R^{FI}(\psi_f)(\dot{p} - \dot{q}(s)) + \begin{bmatrix} 0 & -\dot{\psi}_f \\ \dot{\psi}_f & 0 \end{bmatrix}^T R^{FI}(\psi_f)(p - q(s)) \quad (2.15)$$

Then, taking into account equation (2.12), the plane dynamics are described by:

$$\begin{aligned} \dot{p} &= \begin{bmatrix} \dot{x}_E \\ \dot{y}_E \end{bmatrix} = R^{IF}(\psi) \begin{bmatrix} V \\ 0 \end{bmatrix} + R^{IF}(\psi_w) \begin{bmatrix} W \\ 0 \end{bmatrix} \\ \dot{p} &= \begin{bmatrix} \cos \psi & -\sin \psi \\ \sin \psi & \cos \psi \end{bmatrix} \begin{bmatrix} V \\ 0 \end{bmatrix} + \begin{bmatrix} \cos \psi_w & -\sin \psi_w \\ \sin \psi_w & \cos \psi_w \end{bmatrix} \begin{bmatrix} W \\ 0 \end{bmatrix} \end{aligned} \quad (2.16)$$

And the imaginary target dynamic is described by:

$$\dot{q}(s) = \begin{bmatrix} \dot{s}_x \\ \dot{s}_y \end{bmatrix} = R^{IF}(\psi_f) \begin{bmatrix} \dot{S} \\ 0 \end{bmatrix} = \begin{bmatrix} \cos \psi_f & -\sin \psi_f \\ \sin \psi_f & \cos \psi_f \end{bmatrix} \begin{bmatrix} \dot{S} \\ 0 \end{bmatrix} \quad (2.17)$$

It is worth to note that  $\dot{\psi}_f = \kappa(s)\dot{S}$  as in [20], therefore, (2.15) can be rewritten using (2.16) and (2.17) as:

$$\begin{aligned} \dot{d}_F &= \begin{bmatrix} \cos \psi_f & \sin \psi_f \\ -\sin \psi_f & \cos \psi_f \end{bmatrix} \left( \begin{bmatrix} \cos \psi & -\sin \psi \\ \sin \psi & \cos \psi \end{bmatrix} \begin{bmatrix} V \\ 0 \end{bmatrix} + \begin{bmatrix} \cos \psi_w & -\sin \psi_w \\ \sin \psi_w & \cos \psi_w \end{bmatrix} \begin{bmatrix} W \\ 0 \end{bmatrix} - \right. \\ &\left. \begin{bmatrix} \cos \psi_f & -\sin \psi_f \\ \sin \psi_f & \cos \psi_f \end{bmatrix} \begin{bmatrix} \dot{S} \\ 0 \end{bmatrix} \right) + \begin{bmatrix} 0 & \kappa(s)\dot{S} \\ -\kappa(s)\dot{S} & 0 \end{bmatrix} \begin{bmatrix} \cos \psi_f & \sin \psi_f \\ -\sin \psi_f & \cos \psi_f \end{bmatrix} \left( \begin{bmatrix} x_E \\ y_E \end{bmatrix} - \begin{bmatrix} s_x \\ s_y \end{bmatrix} \right) \end{aligned} \quad (2.18)$$

Defining:  $\tilde{x} = x_E - s_x$ ;  $\tilde{y} = y_E - s_y$ ;  $\tilde{\psi}_1 = \psi - \psi_f$ ;  $\dot{\tilde{\psi}}_1 = \omega - \dot{\psi}_f$ ;

The components of the cross-track error can be rewritten as:

$$e_x = \tilde{x} \cos \psi_f + \tilde{y} \sin \psi_f; \quad e_y = \tilde{y} \cos \psi_f - \tilde{x} \sin \psi_f$$

Finally, equation (2.18) is transformed into:

$$\left. \begin{aligned} \dot{e}_x &= V \cos(\tilde{\psi}_1) + \dot{S}[\kappa(s)e_y - 1] + W \cos(\psi_w - \psi_f) \\ \dot{e}_y &= V \sin(\tilde{\psi}_1) - \kappa(s)e_x\dot{S} + W \sin(\psi_w - \psi_f) \\ \dot{\tilde{\psi}}_1 &= \omega - \kappa(s)\dot{S} \end{aligned} \right\} (2.19)$$

Where:  $\dot{S} = \text{velocity(magnitude)of virtual target}$

$V = \text{airspeed}$   $W = \text{windspeed}$

$\omega = \text{yaw rate}$

$\kappa(s) = \text{curvature of trajectory}$

Therefore, rearranging (2.19):

$$\dot{e} = \begin{bmatrix} \dot{e}_x \\ \dot{e}_y \\ \dot{\tilde{\psi}}_1 \end{bmatrix} = \begin{bmatrix} V \cos(\tilde{\psi}_1) + \dot{S}[\kappa(s)e_y - 1] \\ V \sin(\tilde{\psi}_1) - \kappa(s)e_x\dot{S} \\ \omega - \kappa(s)\dot{S} \end{bmatrix} + \begin{bmatrix} W \cos(\psi_w - \psi_f) \\ W \sin(\psi_w - \psi_f) \\ 0 \end{bmatrix} \quad (2.20)$$

### 2.2.3 Wind Estimation

The contribution of wind disturbance in Serret-Frenet frame is considered as the second term of the right member of equation (2.20), these disturbances are assumed to be bounded:

$$\left\| \frac{d}{dt} W \cos(\psi_w - \psi_f) \right\| \leq \Gamma_1 \quad \left\| \frac{d}{dt} W \sin(\psi_w - \psi_f) \right\| \leq \Gamma_2$$

An auxiliary model without wind disturbances can be introduced.



$$\dot{\hat{e}} = \begin{bmatrix} \dot{\hat{e}}_x \\ \dot{\hat{e}}_y \\ \dot{\hat{\psi}}_1 \end{bmatrix} = \begin{bmatrix} V \cos(\tilde{\psi}_1) + \dot{S}[\kappa(s)e_y - 1] \\ V \sin(\tilde{\psi}_1) - \kappa(s)e_x \dot{S} \\ \omega - \kappa(s)\dot{S} \end{bmatrix} \quad (2.21)$$

Then, an error between models (2.20) and (2.21) is proposed as follows:

$$\tilde{e} = e - \hat{e}$$

$$\dot{\tilde{e}} = \dot{e} - \dot{\hat{e}} = \begin{bmatrix} W \cos(\psi_w - \psi_f) \\ W \sin(\psi_w - \psi_f) \\ 0 \end{bmatrix} \quad (2.22)$$

Where  $e$  is provided by plane measures and  $\hat{e}$  is obtained by a simulated ideal behavior, the term  $\tilde{e}$ , which represents the wind disturbances, can be found using the arbitrary-order exact robust differentiator proposed in [21], which using the auxiliary variables  $(z_0, z_1, z_2)$ , the gains  $(\lambda_0, \lambda_1, \lambda_2)$ , and  $f(t)$  as the function to be derived, the differentiator acquire the form.

$$\dot{z}_0 = v_0$$

$$\dot{z}_1 = v_1$$

$$\dot{z}_2 = v_2$$

Where

$$v_0 = -\lambda_0 |z_0 - f(t)|^{\frac{2}{3}} \text{sign}(z_0 - f(t)) + z_1$$

$$v_1 = -\lambda_1 |z_1 - v_0|^{\frac{1}{2}} \text{sign}(z_1 - v_0) + z_2$$

$$v_2 = -\lambda_2 \text{sign}(z_2 - v_1)$$

Leading that  $z_1 = \dot{z}_0 = f'(t)$ , obtaining the first robust derivative.

Note that the  $\lambda$  gains are chosen using the bounds  $\Gamma_i$  ( $i = 1,2$ ), being these bounds given constants. At larger values of  $\lambda$ 's, the convergence of the differentiator is faster, and the sensitivity to input noises and the sampling step is higher.

Hence, the parameters  $\lambda$  are chosen as follows.

$$\lambda_0 = 3\Gamma_i^{1/3}$$

$$\lambda_0 = 1.5\Gamma_i^{1/2}$$

$$\lambda_0 = 1.1\Gamma_i$$

## 2.2.4 Path following Control.

The path following control will be carried by an outer-loop controller while the orientation control of the vehicle will be made by an inner-loop controller; The outer-loop controller is based on a control law similar to the law used for a submarine in [19], or the law used for a small airplane in [20], both of them examples of the carrot-chasing algorithm which is wanted to improve.

An approaching angle ( $\psi_a$ ) is induced to follow the desired trajectory, parameterized by the gain  $k_\delta > 0$  (In simulation  $k_\delta = .8$ ).

$$\delta(e_y) = -\psi_a \frac{e^{2k_\delta e_y} - 1}{e^{2k_\delta e_y} + 1} \quad 0 < \psi_a < \frac{\pi}{2}$$

Where the sigmoid function is bounded and differentiable with respect to the error  $e_y$ . This approaching angle will depend on the error  $e_y$  and will be the yaw angle that the plane will need to take in order to follow the path.

Observe that if

$$e_y = 0 \xrightarrow{\text{yields}} \delta(e_y) = 0$$

Also

$$e_y > 0 \xrightarrow{\text{yields}} \delta(e_y) < 0 \quad e_y < 0 \xrightarrow{\text{yields}} \delta(e_y) > 0$$

Meaning that if the plane is at the left of the trajectory, it will turn at the right and viceversa, which leads to:  $e_y \delta(e_y) \leq 0 \quad \forall e_y$ .

Then, the real model described in equation (2.20), can be written as

$$\left. \begin{aligned} \dot{e}_x &= V \cos(\tilde{\psi}_1) + \dot{S}[\kappa(s)e_y - 1] + W_x \\ \dot{e}_y &= V \sin(\tilde{\psi}_1) - \kappa(s)e_x \dot{S} + W_y \\ \dot{\tilde{\psi}}_1 &= \omega - \kappa(s)\dot{S} \end{aligned} \right\} \quad (2.23)$$

Where  $W_x = W \cos(\psi_w - \psi_f)$  and  $W_y = W \sin(\psi_w - \psi_f)$  are known thanks to the arbitrary-order exact robust differentiator.

Proposing the Lyapunov function:

$$V(e_x, e_y, \tilde{\psi}_1) = \frac{1}{2}e_y^2 + \frac{1}{2}(\tilde{\psi}_1 - \delta(e_y))^2 + \frac{1}{2}e_x^2 \quad (2.24)$$

Obtaining its derivative and introducing system dynamics:

$$\dot{V}(e_x, e_y, \tilde{\psi}_1) = e_y \dot{e}_y + (\tilde{\psi}_1 - \delta(e_y))(\dot{\tilde{\psi}}_1 - \dot{\delta}(e_y)) + e_x \dot{e}_x$$

$$\dot{V}(e_x, e_y, \tilde{\psi}_1) = (\tilde{\psi}_1 - \delta(e_y))(\omega + \mu) + e_x(V \cos \tilde{\psi}_1 + W_x - \dot{S}) + e_y(V \sin(\delta(e_y)))$$

Where:

$$\begin{aligned} \mu &= -\kappa(s)\dot{S} - \dot{\delta}(e_y) + e_y \left( \frac{V(\sin \tilde{\psi}_1 - \sin \delta(e_y)) + W_y}{(\tilde{\psi}_1 - \delta(e_y))} \right) \\ \dot{\delta}(e_y) &= \frac{\partial \delta(e_y)}{\partial e_y} \frac{\partial e_y}{\partial t} = -\frac{4\psi_a k_\delta e^{2k_\delta e_y}}{(e^{2k_\delta e_y} + 1)^2} e_y \\ &= -\frac{4\psi_a k_\delta e^{2k_\delta e_y}}{(e^{2k_\delta e_y} + 1)^2} (V \sin \tilde{\psi}_1 + W_y - \kappa(s)e_x \dot{S}) \end{aligned}$$

Then, taking  $\dot{S}$  y  $\omega$  as control inputs, these expressions are proposed:

$$\dot{S} = V \cos \tilde{\psi}_1 + W_x + k_S e_x$$

$$\omega = -\mu - k_\omega (\tilde{\psi}_1 - \delta(e_y))$$

Rewriting Lyapunov function with some gain parameters  $k_\omega > 0$ ,  $k_S > 0$  (In simulation  $k_\omega = .7$  and  $k_S = 5$ ):

$$\dot{V}(e_x, e_y, \tilde{\psi}_1) = -k_\omega (\tilde{\psi}_1 - \delta(e_y))^2 - k_S e_x^2 + V e_y \sin(\delta(e_y)) \leq 0 \quad (2.25)$$

Where the term  $V e_y \sin \delta(e_y)$  will have the form shown in Fig 2.5:



Fig. 2.5: Graphic of the term  $V e_y \sin \delta(e_y)$ .

Then, LaSalle's invariance principle is used to prove the system convergence.

Let  $\Omega$  be a compact (closed and bounded) set with the property that every solution of the system (2.23) which starts in  $\Omega$  remains in  $\Omega$  for all future time. Let  $V: \Omega \rightarrow \mathbb{R}$  (equation 2.24) be a continuously differentiable function such that  $\dot{V} \leq 0$  in  $\Omega$  (equation 2.25). Let  $E$  be the set of all points in  $\Omega$  where  $\dot{V}(e_x, e_y, \tilde{\psi}_1) = 0$ . Let  $M$  be the largest invariant set in  $E$ . Then every solution starting in  $\Omega$  approaches  $M$  as  $t \rightarrow \infty$ .

The proof relies on LaSalle's theorem [22]. Consider the system (2.23) and the radially unbounded Lyapunov function candidate (2.24). Let us define  $\Omega = \{V(e_x, e_y, \tilde{\psi}_1) \leq a\}$ , where  $a \in \mathbb{R}^+$ . Define the set  $E = \{[e_x \ e_y \ \tilde{\psi}_1]^T \in \Omega \ : \ \dot{V}(e_x, e_y, \tilde{\psi}_1) = 0\}$ .

Equivalently, the expression  $\dot{V}(e_x, e_y, \tilde{\psi}_1) = 0$  means that  $e_x = e_y = 0$  and  $\tilde{\psi}_1 = \delta(e_y)$ , and as  $\delta(e_y)$  is a function dependent on the error  $e_y$ , is easy to verify that every trajectory converges to 0 as  $t \rightarrow \infty$ . Hence, the following limits are true.

$$\lim_{t \rightarrow \infty} e_x \rightarrow 0 \qquad \lim_{t \rightarrow \infty} e_y \rightarrow 0 \qquad \lim_{t \rightarrow \infty} \tilde{\psi}_1 = \delta(e_y) = 0$$

Furthermore, regarding to the lateral movement that will allow the plane to change its position, it is considered that the lateral movement is induced by a roll angle variation (See Appendix B), that is why the roll angle needs to be delimited in magnitude ( $|\phi| \leq \phi_{max}$ ); heading rate is denoted by:

$$\omega = \frac{g}{V} \tan \phi$$

Simultaneously, the inner-loop controller, responsible for the orientation, will have the task to make that the airplane goes from an initial roll angle to a desired roll angle. So that, using the roll dynamic of the plane's complete model seen in the first chapter:

$$\ddot{\phi} = C_8 V^2 + C_{10} \tau_\phi$$

Where the control  $u_\phi$  can be introduced in the model as:

$$\tau_\phi = \frac{u_\phi}{C_{10}} - C_8 V^2$$

Leading to a double integrator:

$$\ddot{\phi} = u_\phi$$

Which will extend the path following equations to:

$$\dot{e}_x = V \cos \tilde{\psi}_1 + \dot{S}[\kappa(s)e_y - 1] + W_x$$

$$\dot{e}_y = V \sin \tilde{\psi}_1 - \kappa(s)e_x \dot{S} + W_y$$

$$\dot{\tilde{\psi}}_1 = \frac{g}{V} \tan \phi - \kappa(s) \dot{S}$$

$$\dot{\phi} = p$$

$$\dot{p} = u_\phi$$

$$p = \text{roll rate}$$

In this equations, the controller obtained in the outer-loop controller will play a key role, as it will be considered as the desired heading rate  $\omega_d$  for the control  $u_\phi$ .

So, from relation of heading rate  $\omega = \frac{g}{V} \tan \phi$  it is obtained:

$$\phi = \tan^{-1} \left( \frac{V}{g} \omega \right)$$

And thanks to the outer-loop controller:

$$\phi^d = \tan^{-1} \left( \frac{V}{g} \omega_d \right)$$

Then, considering that the inner-loop controller applies a backstepping method:

It is wanted that  $\phi \rightarrow \phi^d$

Defining the first error  $e_1 = \phi - \phi^d$

And its derivative  $\dot{e}_1 = p - p^d$

Using a Lyapunov function:

$$V_1 = \frac{1}{2} e_1^2$$

$$\dot{V}_1 = e_1 \dot{e}_1 = e_1 (p - p^d)$$

Proposing:  $p^v = p^d - e_1$  and its derivative  $\dot{p}^v = \dot{p}^d - \dot{e}_1 = \dot{p}^d - p + p^d$

Leading to:  $p^d = p^v + e_1$

$$\dot{V}_1 = e_1(p - p^v - e_1) = -e_1^2 + e_1(p - p^v)$$

Defining second error  $e_2 = p - p^v$  and its derivative  $\dot{e}_2 = \dot{p} - \dot{p}^v = u_\phi - \dot{p}^v$

Rewriting first Lyapunov function:

$$\dot{V}_1 = -e_1^2 + e_1 e_2$$

Using a second Lyapunov function

$$V_2 = \frac{1}{2} e_2^2$$

$$\dot{V}_2 = e_2 \dot{e}_2 = e_2(u_\phi - \dot{p}^v)$$

Proposing the control law:

$$u_\phi = -e_1 - e_2 + \dot{p}^v$$

$$\dot{V}_2 = e_2(-e_1 - e_2 + \dot{p}^v - \dot{p}^v) = -e_2^2 - e_1 e_2$$

Then, adding the Lyapunov functions.

$$V_T = V_1 + V_2 = \frac{1}{2} e_1^2 + \frac{1}{2} e_2^2$$

$$\dot{V}_T = -e_1^2 - e_2^2 + e_1 e_2 - e_1 e_2$$

$$\dot{V}_T = -e_1^2 - e_2^2$$

Developing control law:

$$u_\phi = -e_1 - e_2 + \dot{p}^v$$

$$= -\phi + \phi^d - p + p^v + \dot{p}^d - p + \dot{p}^d$$

$$= -\phi - \phi - p - p + \phi^d + \phi^d + p^d + p^d + \dot{p}^d$$

$$u_\phi = -2(\phi - \phi^d) - 2(p - p^d) + \dot{p}^d$$

Which leads to  $\phi \rightarrow \phi^d$  and  $p \rightarrow p^d$

So, the Lyapunov total function will be:

$$W = \frac{1}{2}e_1^2 + \frac{1}{2}e_2^2 + \frac{1}{2}e_y^2 + \frac{1}{2}(\tilde{\psi}_1 - \delta(e_y))^2 + \frac{1}{2}e_x^2$$

$$\dot{W} = -e_1^2 - e_2^2 - k_\omega (\tilde{\psi}_1 - \delta(e_y))^2 - k_S e_x^2 + V e_y \sin \delta(e_y) \leq 0$$

Where:

$$e_1 = \phi - \phi^d$$

$$e_2 = p - p^d + \phi - \phi^d$$

Assuring stability.

The simulation of this inner-controller gives the following results (Fig. 2.6).

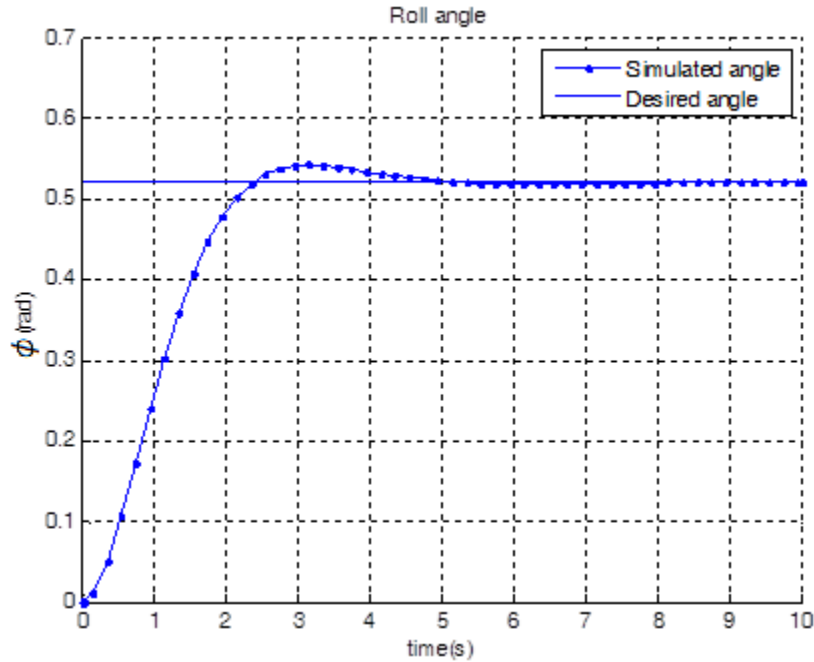


Fig. 2.6: Backstepping roll angle simulation.



## Chapter 3.

### Prototype.

In order to obtain experimental data, a small modified RC plane is used in this work, the model is called Twinstar II, and its characteristics are shown in the following table:

Wingspan	1.42 <i>m</i>
Wing Area	.43 <i>m</i> <sup>2</sup>
Fuselage	1.02 <i>m</i>
Weight	1.44 <i>kg</i>
Price	100 €

Here in Fig. 3.1 is shown the original plane, and in Fig. 3.2 and Fig. 3.3 is shown after modifications.



Fig. 3.1: Original airplane.



Fig. 3.2: Modified airplane.



Fig. 3.3: Modified airplane(Upper view).

A LiPo battery of  $5000mA$  ,  $11.1v$  , with a weight of  $390g$  and price of  $25\epsilon$  is used as the power supply for the plane and avionics, as the propulsion, the plane was provided with two out-runner brushless motors Roxxy 2827-34, which have a weight of  $57g$  and a price of  $31.5\epsilon$  each, both components are shown in Fig. 3.4.



Fig. 3.4: LiPo battery and brushless motor.

A Pitot tube is used to measure the dynamic pressure, which according to the fluid dynamics, allows us to calculate the relative velocity of the plane with respect to the air mass surrounding the plane (airspeed) with the equation:

$$v = \sqrt{\frac{2q}{\rho}}$$

Where  $q$  is the dynamic pressure,  $\rho$  the air density and  $v$  the airspeed.

The model used is the Eagle Tree airspeed Micro Sensor V3 (see Fig. 3.5), and is mounted in the wing in order to do not have big quantities of noise in the measure; this noise can be induced by the air flow of the motors or air flow modifications caused by the plane's structure.



Fig. 3.5: Pitot tube.

The autopilot used is the PX4 [23] (see Fig. 3.6), this autopilot was chosen because of its size, sensor availability, peripherals supported, the expansion ports already developed, and compatibility with several platforms (in case that a change of vehicle is wanted). Other aspects that are important to mention are the cheap price in relation

with other autopilots such as the Micro pilot family, the U-Pilot One board, Ardupilot, DJI(Wookong M Waypoint), Zero UAV (YS-X4/X6), uThere (Ruby), and finally, for the huge difference that the PX4 has an Open Source software.

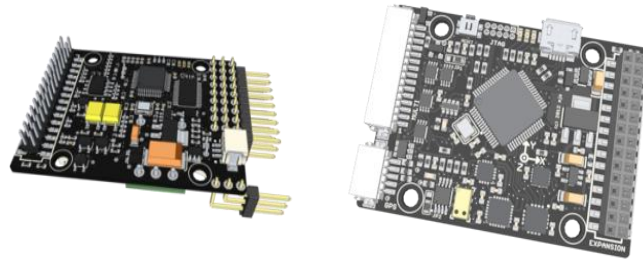


Fig. 3.6: PX4 autopilot with the ports expansion.

This autopilot has already integrated inertial sensors (gyroscopes, accelerometers and magnetometers) as well as a barometric pressure sensor (altimeter), components shown in Fig. 3.7.

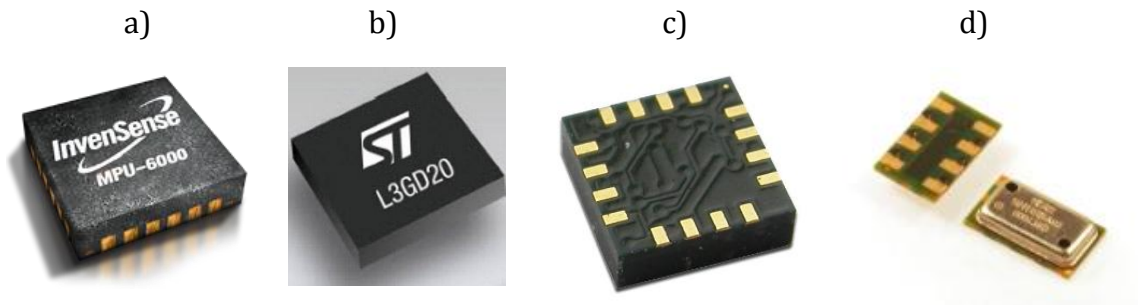


Fig. 3.7: Sensors in the PX4 autopilot.

	Type of sensor	Precision
a)	3-axis gyroscope 3-axis accelerometer	$\pm 250, \pm 500, \pm 1000, \text{ and } \pm 2000^\circ/\text{sec}$ $\pm 2g, \pm 4g, \pm 8g \text{ and } \pm 16g.$
b)	3-axis gyroscope	$\pm 250, \pm 500 \text{ and } \pm 2000^\circ/\text{sec}$
c)	3-axis magnetometer	Milli-gauss Field Resolution in $\pm 8$ Gauss Fields $1^\circ \text{ to } 2^\circ$ Compass Heading Accuracy
d)	Barometric pressure	10cm

A GPS is also used to obtain the position of the plane in the inertial frame. The GPS is mounted as near as possible of the mass center of the vehicle in order to be more precise in the practice experimentation. The model used is the 3DR uBlox LEA-6 H High-Performance Receiver (see Fig. 3.8), which has a total size of 38 x 38 x 8.5 mm and a weight of 16.8 g; The GPS data is updated at a rate of 5Hz.



Fig. 3.8: GPS model.

As the inertial frame on the earth is taken as a flat surface and the GPS gives the measures of the position in LLA, which means latitude, longitude and altitude ( $\gamma, \lambda, h$ ), and the measurements of the velocity are provided in a NED (north, east, down) frame (see Fig. 3.9), some transformations are needed, first, a reference point in the earth is taken and is described by the latitude ( $\gamma_{ref}$ ), longitude ( $\lambda_{ref}$ ) and altitude ( $h_{ref}$ ), then, when the GPS gives the position data, the simplest transformation to the NED frame is done:

$$x = R(\gamma - \gamma_{ref})$$

$$y = R \cos(\gamma_{ref})(\lambda - \lambda_{ref})$$

$$z = -(h - h_{ref})$$

where R is the earth's radius.

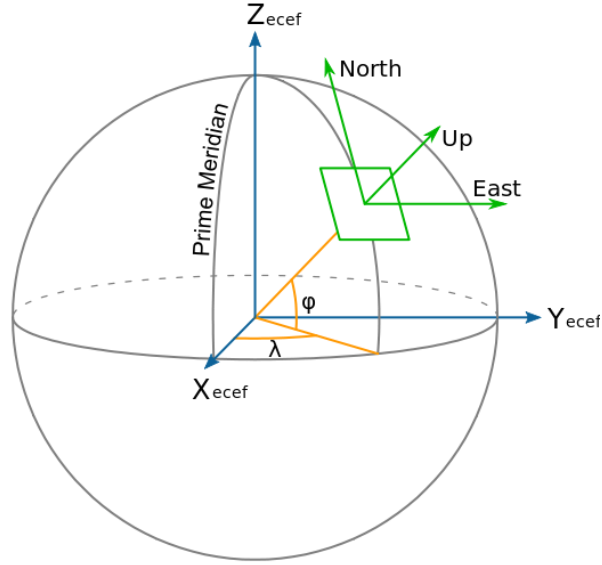


Fig. 3.9: Frames on earth.

Once that position and velocity is in the NED frame, this is considered to be in a flat surface.

In order to return from this “local” position to the “global” position (from NED to LLA), instead of using the method were the earth is taken as an ellipsoid with certain values of eccentricity, flattening, and distances of semi-major and semi-minor axes given by the WGS84 (Geodetic World System in 1984) and go from the NED frame to the ECEF frame, and then to the LLA frame, a simpler Gnomonic projection is used, this perspective projection of the globe from the center onto a plane tangent to the surface and viceversa is describe by the following equations:

$$\lambda = \left\{ \begin{array}{ll} \lambda_{ref} + \tan^{-1} \left( \frac{x \sin c}{c \cos \gamma_{ref} \cos c - y \sin \gamma_{ref} \sin c} \right) & \text{for } \gamma_{ref} \neq 90^\circ \\ \lambda_{ref} + \tan^{-1} \left( -\frac{x}{y} \right) & \text{for } \gamma_{ref} = 90^\circ \\ \lambda_{ref} + \tan^{-1} \left( \frac{x}{y} \right) & \text{for } \gamma_{ref} = -90^\circ \end{array} \right\}$$

$$\gamma = \sin^{-1} \left( \cos c \sin \gamma_{ref} + \frac{y \sin c \cos \gamma_{ref}}{c} \right)$$

$$c = \sqrt{x^2 + y^2}$$

Where  $c$  is the angular distance of the given point from the reference point of the projection, for more information please refer to [24] .

The data transmission is done by an Xbee module (see Fig. 3.10); data is transmitted during the flight to the computer in order to visualize parameters of the plane or of the flight, despite of the fact that these parameters are visualized, data coming from the sensors are stored in a micro SD card in each flight.



Fig. 3.10: Xbee modem.

The ground station used is the QGroundControl (see reference [25]), which is a next generation micro air vehicle ground control station which allows the user to visualize variables such as plane angles and rates, GPS measures, airspeed given by Pitot tube. The base code was developed 2009-2010 in the PIXHAWK Project at ETH Zurich by Lorenz Meier. It is since 2010 under community development with a wide range of projects and individuals.

In order to flight manually the plane, the radio transmitter and receiver, *Futaba T6EX* and *Futaba R617FS* respectively, are used, then the PWM (Pulse width modulation) signal from the receiver is transformed into a PPM (Pulse position modulation) signal via a PPM encoder, subsequently, the signal is acquired by the PX4.

In order to have control of the surfaces in the plane such as ailerons, elevator and rudder, servo motors are used.

Here in Fig. 3.11 is shown a block diagram of the prototype hardware, showing the interconnection between the devices described in this section and giving an overview of the data flow.

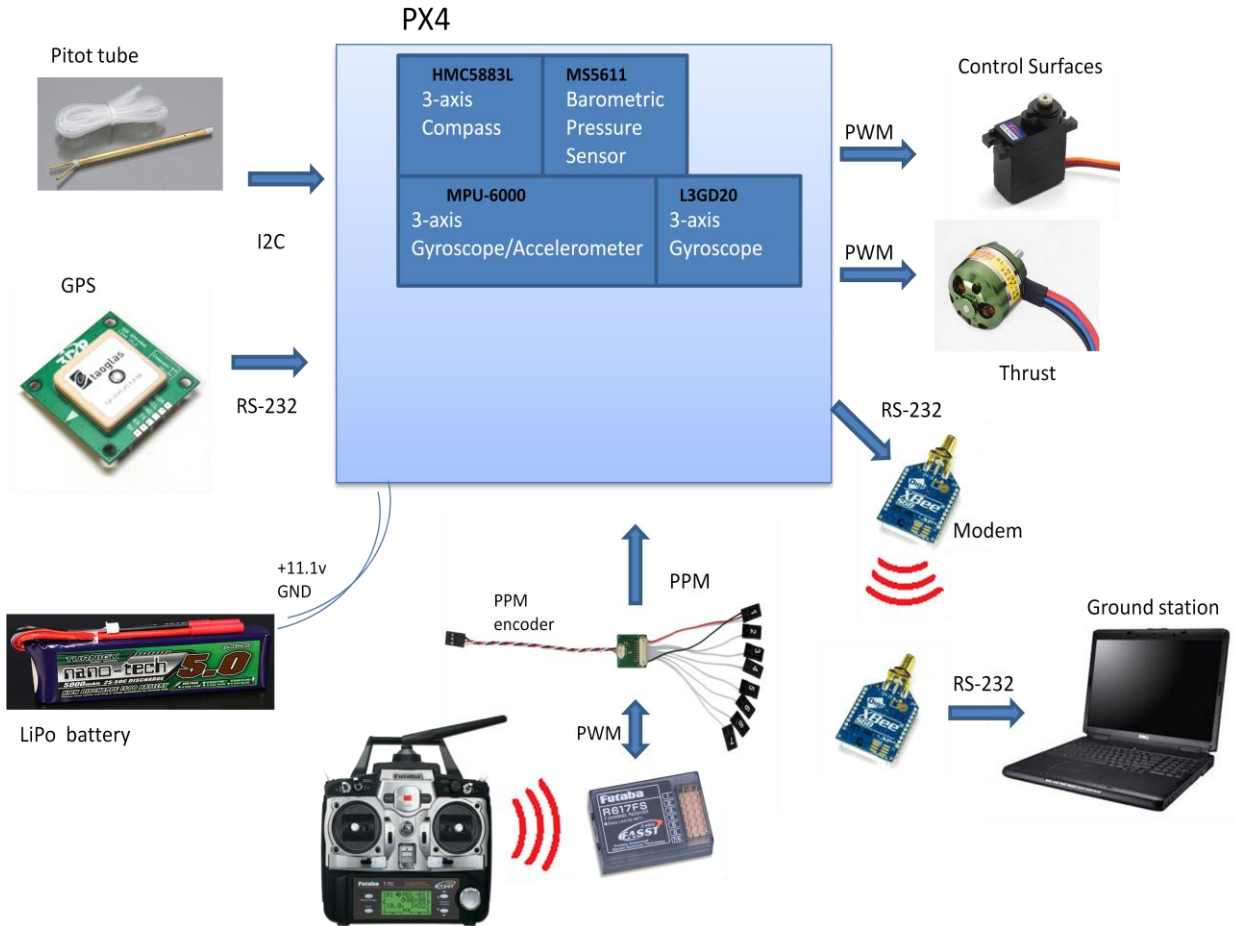


Fig. 3.11: PX4 autopilot with peripherals and outputs.



## Chapter 4.

### Results.

#### 4.1 Simulation Results.

The simulations shown in this part are regarding the second approach showed in Section 2.2 to perform path following, and the following results were obtained.

As the first part of simulation, a time independent trajectory was needed to run simulations, a circular path with radius of 50m was chosen, therefore, using the reparametrization theory and making the trajectory construction dependent on the arclength, it means, on the waypoints reached by the plane (which depends by definition on its velocity, and so on in the velocity error with respect to the imaginary particle's velocity), it is obtained the path of Fig. 4.1.

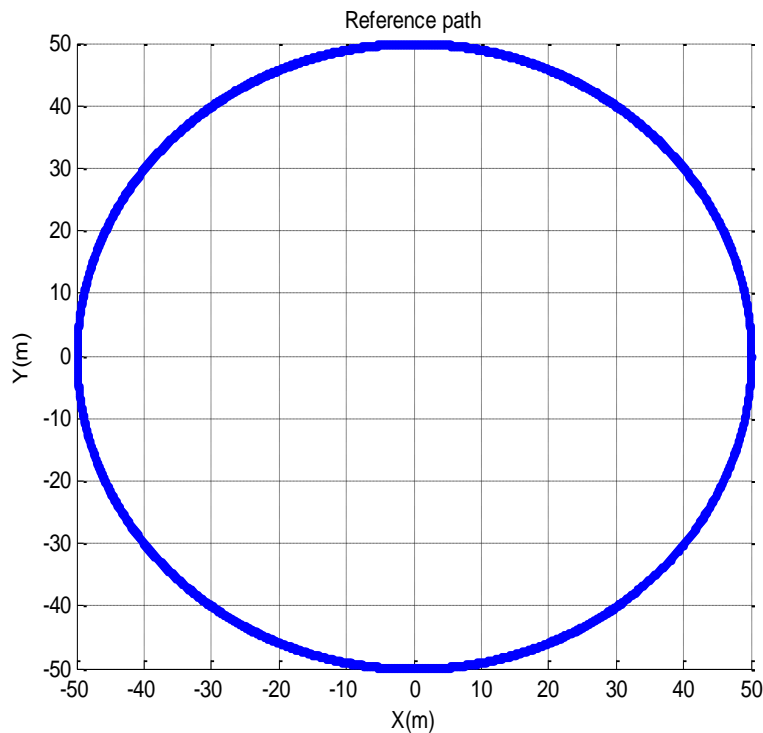


Fig. 4.1: Reference path.

Then, the following part of simulation was the auxiliary system (2.21) used as an ideal model, and the real model (2.20) with disturbances included.

$$\begin{bmatrix} \dot{\tilde{e}}_x \\ \dot{\tilde{e}}_y \\ \dot{\tilde{\psi}}_1 \end{bmatrix} = \begin{bmatrix} V \cos(\tilde{\psi}_1) + \dot{S}[\kappa(s)e_y - 1] \\ V \sin(\tilde{\psi}_1) - \kappa(s)e_x \dot{S} \\ \omega - \kappa(s)\dot{S} \end{bmatrix}$$

$$\dot{e} = \begin{bmatrix} \dot{e}_x \\ \dot{e}_y \\ \dot{\psi}_1 \end{bmatrix} = \begin{bmatrix} V \cos(\tilde{\psi}_1) + \dot{S}[\kappa(s)e_y - 1] \\ V \sin(\tilde{\psi}_1) - \kappa(s)e_x \dot{S} \\ \omega - \kappa(s)\dot{S} \end{bmatrix} + \begin{bmatrix} W \cos(\psi_w - \psi_f) \\ W \sin(\psi_w - \psi_f) \\ 0 \end{bmatrix}$$

The plane velocity was chosen of 15 m/s, and the curvature, as a constant value for being a circular path, defined as 0.02. Furthermore, the plane is assumed to have a wingspan of 2m and flight at 150m height throughout simulations.

The wind perturbation on each axe is proposed via Dryden's wind model, and are shown in Fig. 4.2 and Fig. 4.3.

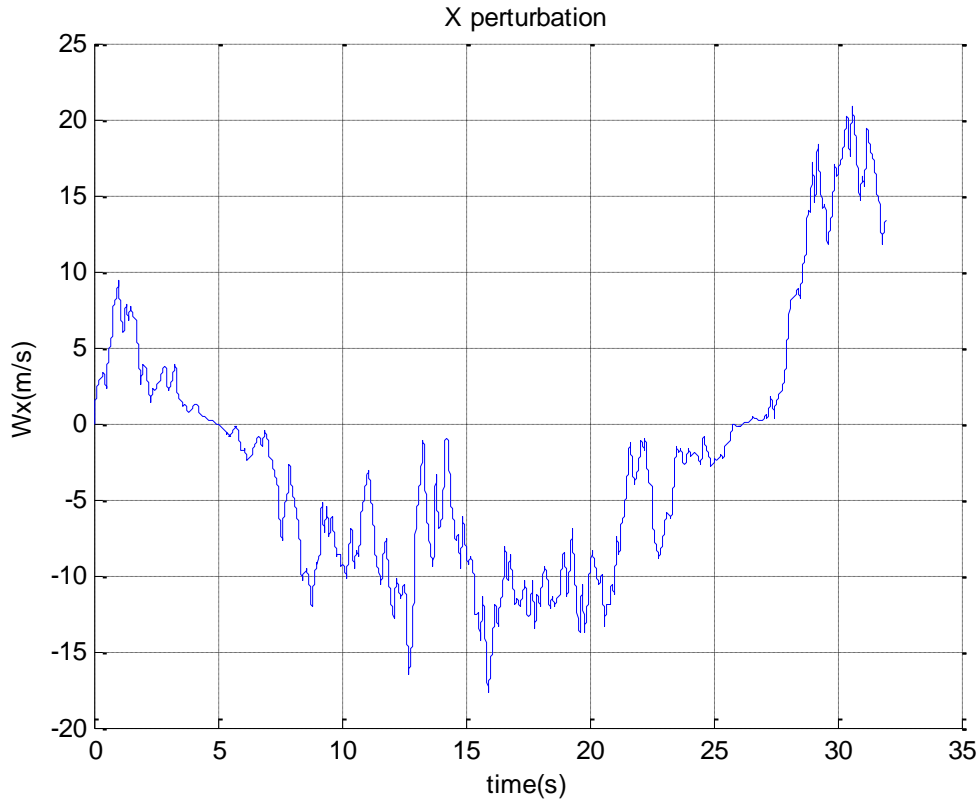


Fig. 4.2: Disturbance in  $x$ .

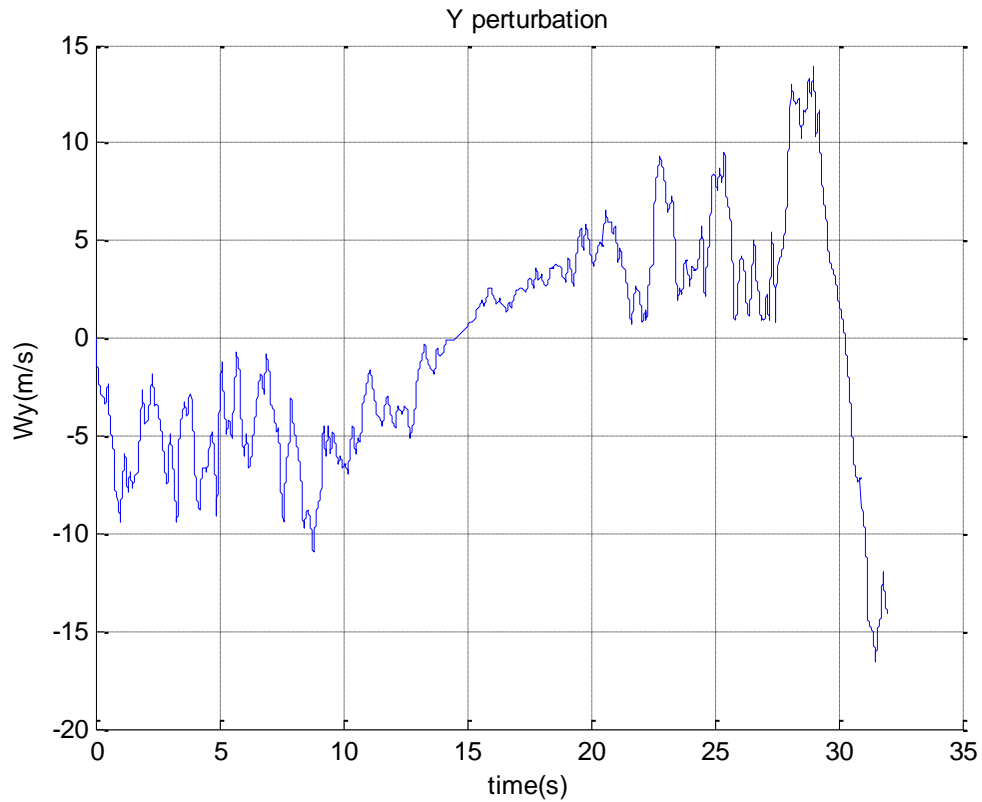


Fig. 4.3: Disturbance in  $y$ .

Once that a disturbance, reference path, and the two models of path following are defined, the Lyapunov based control law derived from the theory can be introduced.

The corresponding trajectory errors of the path following method are measured in the Serret-Frenet frame, meaning that these measures correspond, the first one, to the error perpendicular to the trajectory tangent line, and the other measure, to the velocity error, assuring that as these errors tend to zero, the plane is following the trajectory as it should. The results are shown in Fig. 4.4-Fig. 4.7.

According to the theory, in order to obtain the wind estimation, the errors are measured in the real and ideal systems, i.e., with and without wind models, the Fig. 4.4 and Fig. 4.5, express the  $x$  error on each system respectively.

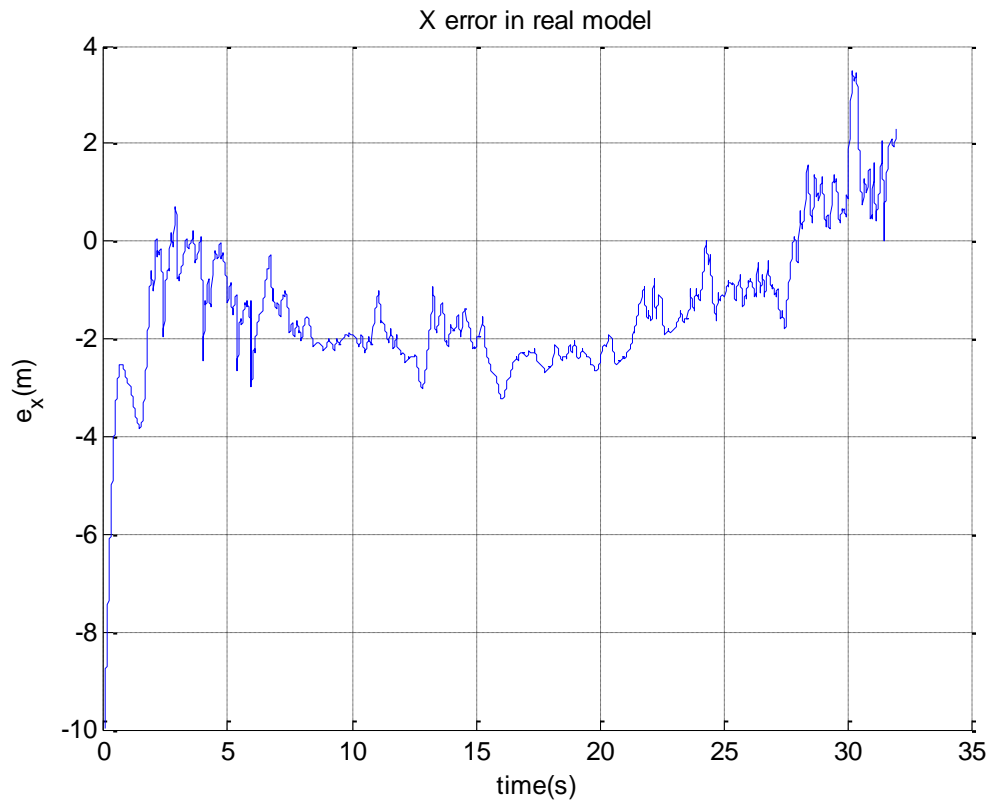


Fig. 4.4:  $x$  error in real model.

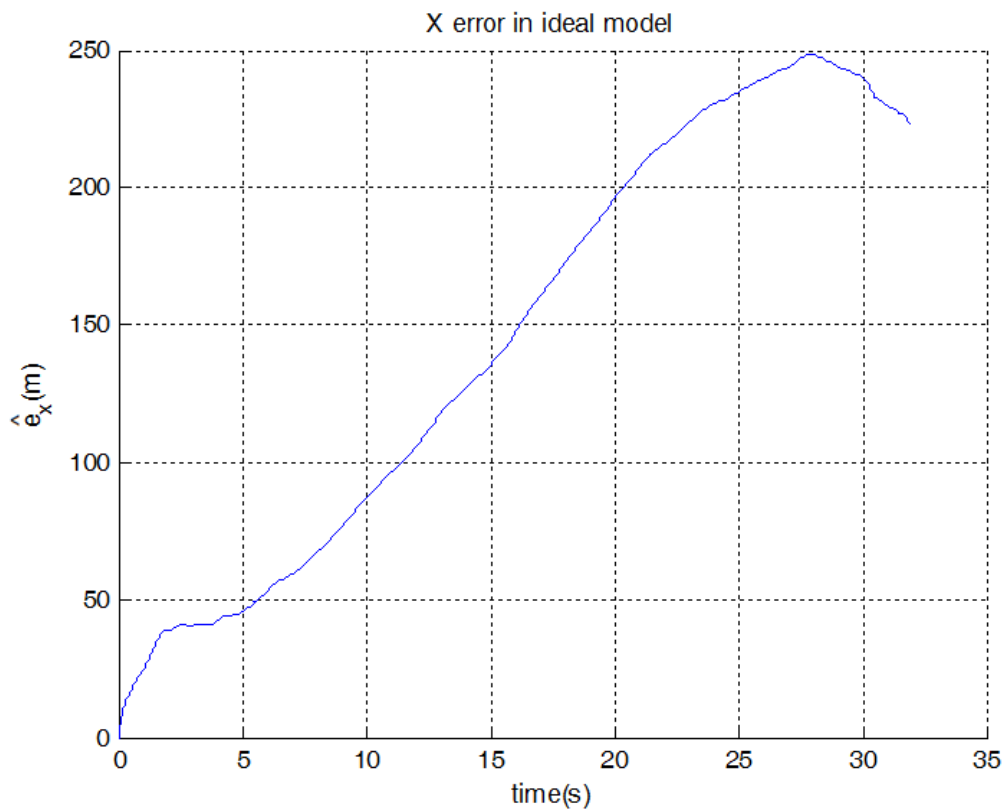


Fig. 4.5:  $x$  error in ideal model.

While the imaginary particle is followed by the plane, the Fig. 4.6 and Fig. 4.7, express the velocity error in the Serret-Frenet frame in the real and ideal model respectively

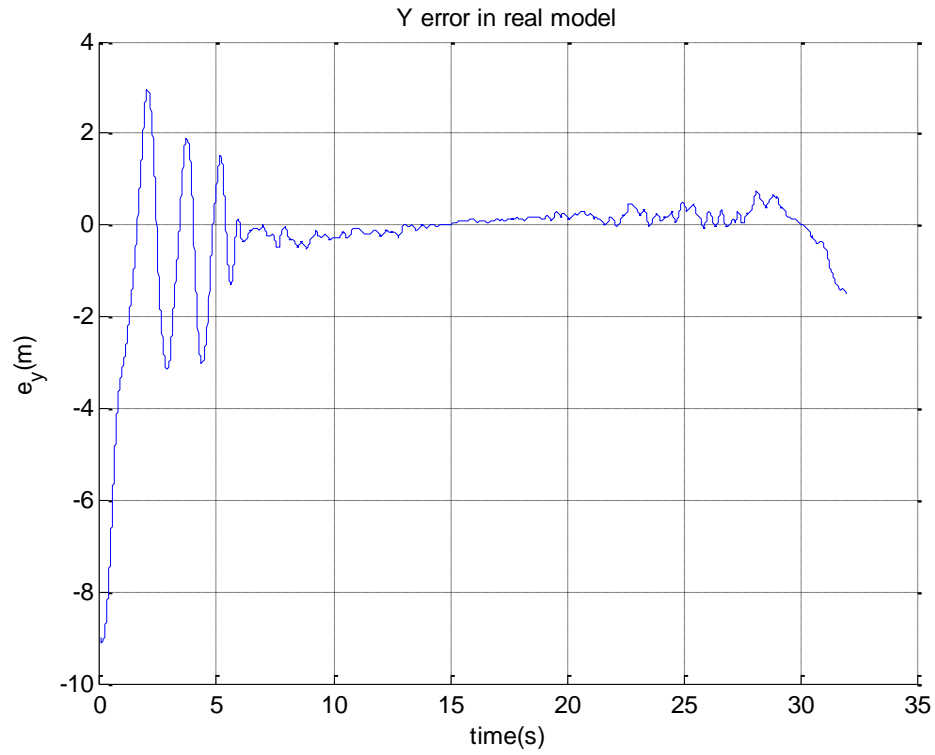


Fig. 4.6: y error in real model.

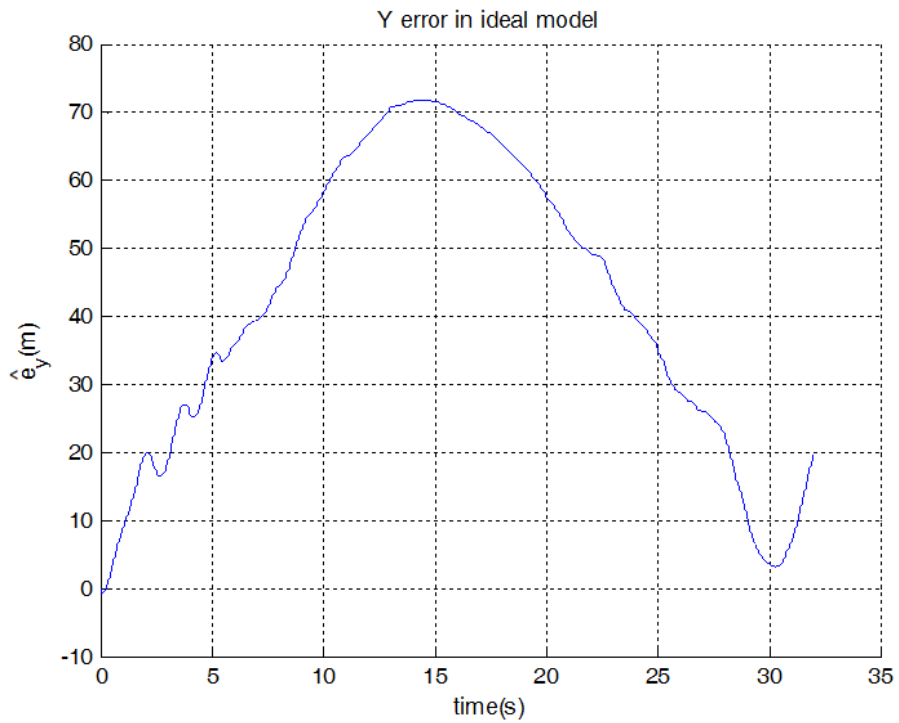


Fig. 4.7: y error in ideal model.

After these results are obtained, each error of each axe is compared, the errors from the ideal model are subtracted from the real model, and according to the theory given in Section 2.2.3, concerning to the wind estimation part, this action provides the term  $\tilde{e}$  from equation (2.22), which is shown in Fig. 4.8 and 4.9, then obtaining its derivative using the arbitrary-order exact robust differentiator presented in Section 2.2.3, the disturbance terms for each axe are obtained and shown in Fig. 4.10 and 4.11.

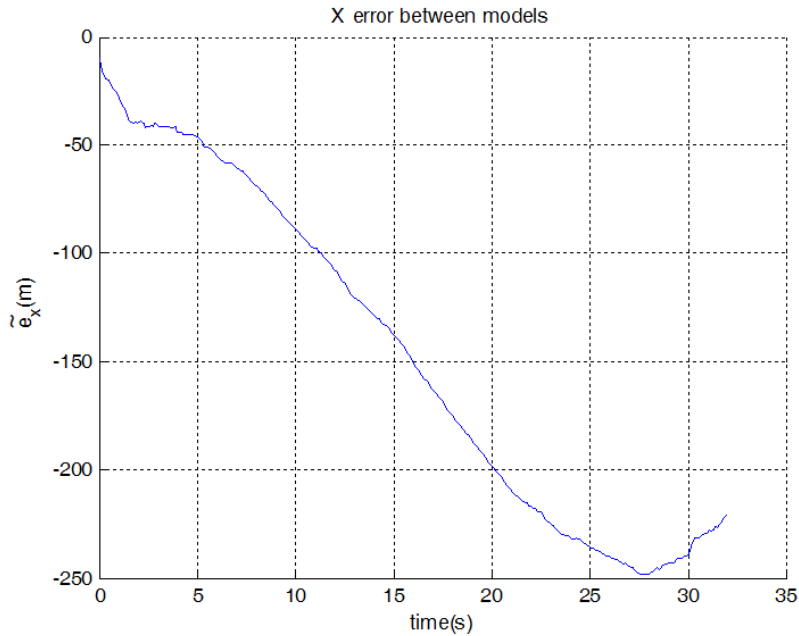


Fig. 4.8:  $x$  error between real and ideal models.

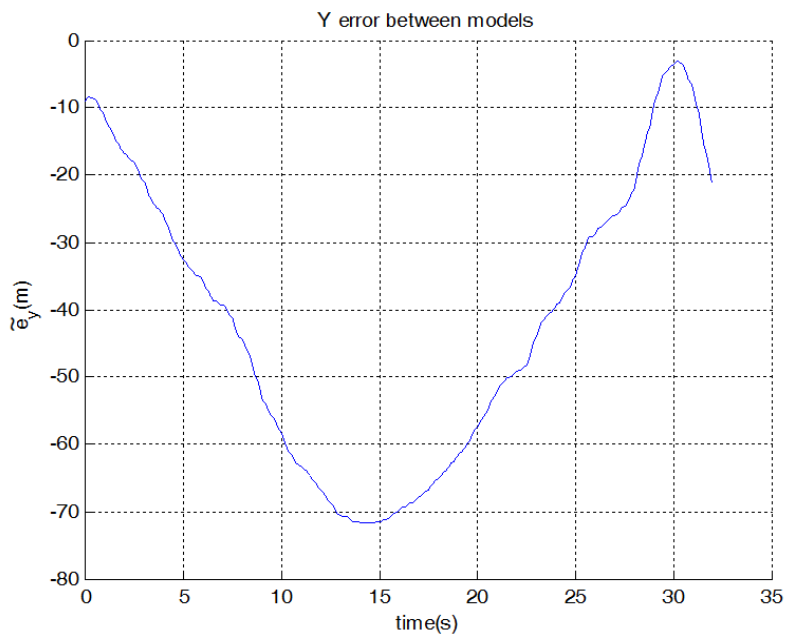


Fig. 4.9:  $y$  error between real and ideal models.

Note that due to the signal processing, a delay is introduced in the wind estimates

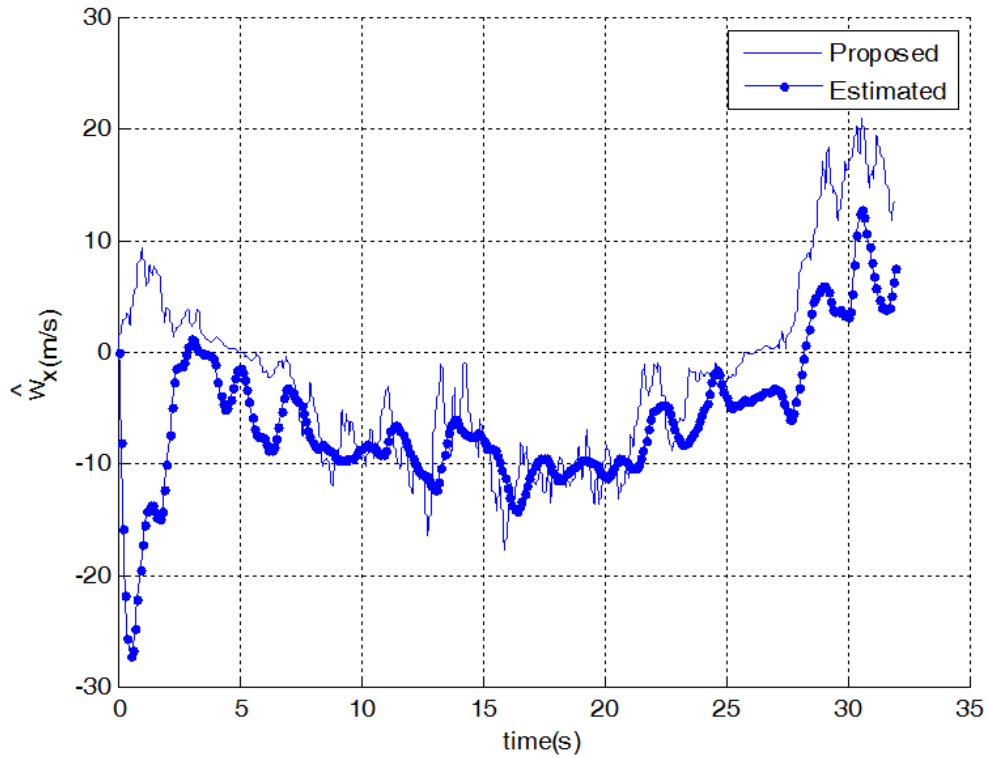


Fig. 4.10: Estimation of the disturbance in  $x$  axe.

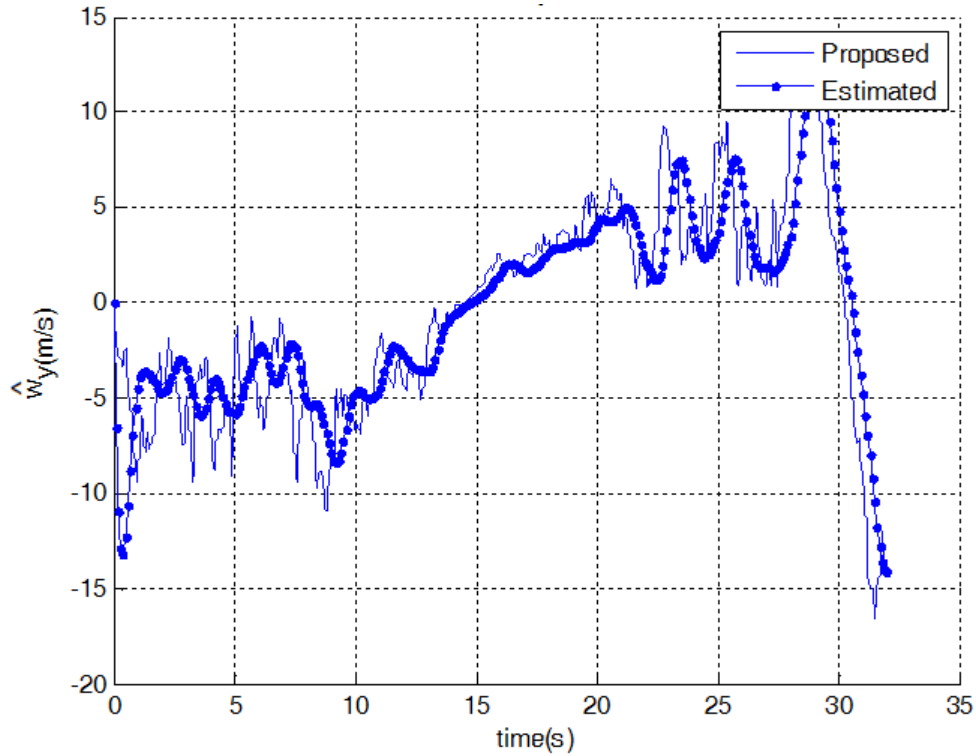


Fig. 4.11: Estimation of the disturbance in  $y$  axe.

Finally, adding the wind estimation to the control law presented in Section 2.2.4, the trajectory of the plane obtained in the simulation is shown in the Fig. 4.12.

At the initial time, the reference path begins at the coordinates  $x = 50m$ ,  $y = 0m$ , with an angle of  $90^\circ$ , and the initial plane position is  $x = 59m$ ,  $y = -10m$  with an angle of  $75^\circ$ .

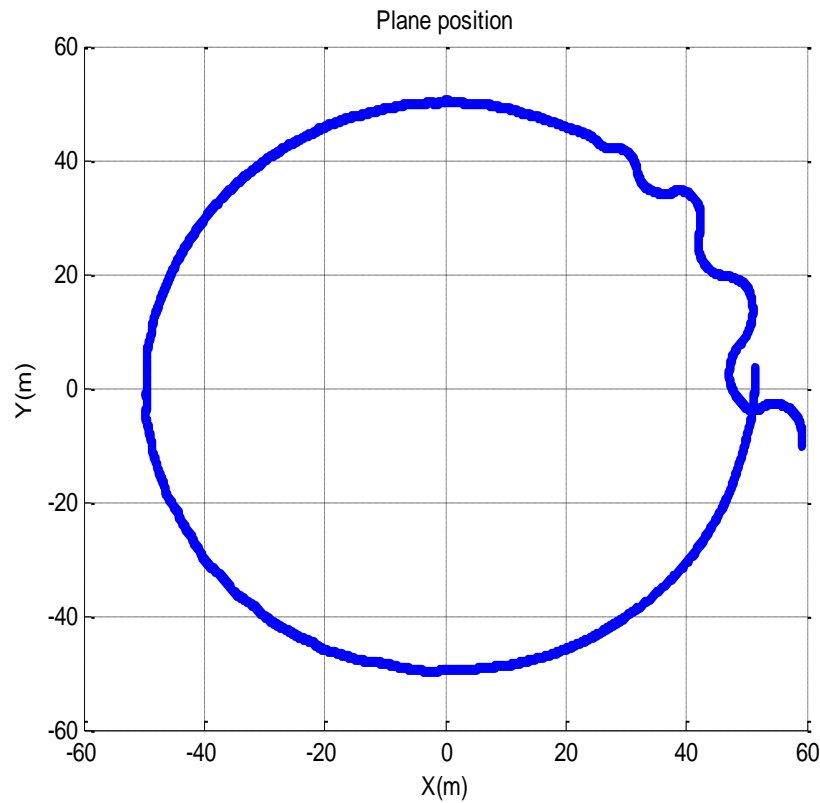


Fig. 4.12: Plane trajectory.



## 4.2 Experimental Results.

After some flights realized with the first approach implemented in the onboard electronics, some graphics were obtained from the data measured by the plane during the flights, altitude is not controlled in this algorithm but is plotted anyways in order to give an idea of the altitude of the plane in tests.

The first flight began with manual control, which gives the opportunity to avoid crashes during takeoff and landing, and launch the control algorithm at an altitude which allows the pilot to change mode between manual and automatic if an error takes place.

The Fig. 4.13 shows the stage of takeoff. A strong curve is done before the change between manual an automatic flight in order to identify properly in the videos the beginning of the automatic flight, the curve can be appreciated in the bottom left of the figure.

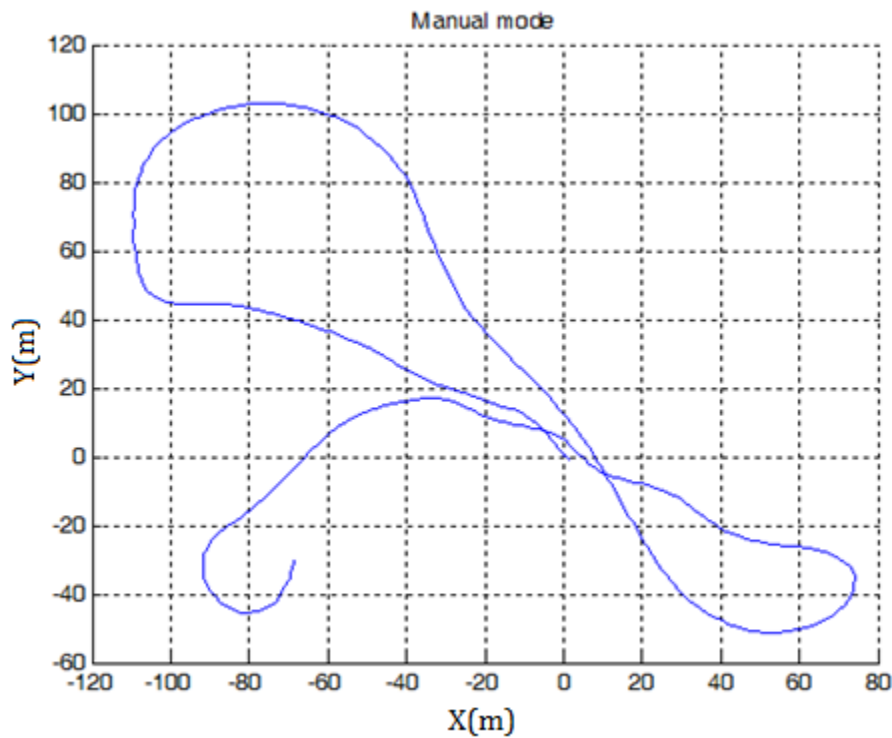


Fig. 4.13: Trajectory in manual mode.

The automatic flight trajectory, which is a loiter path, can be seen in the Fig. 4.14.

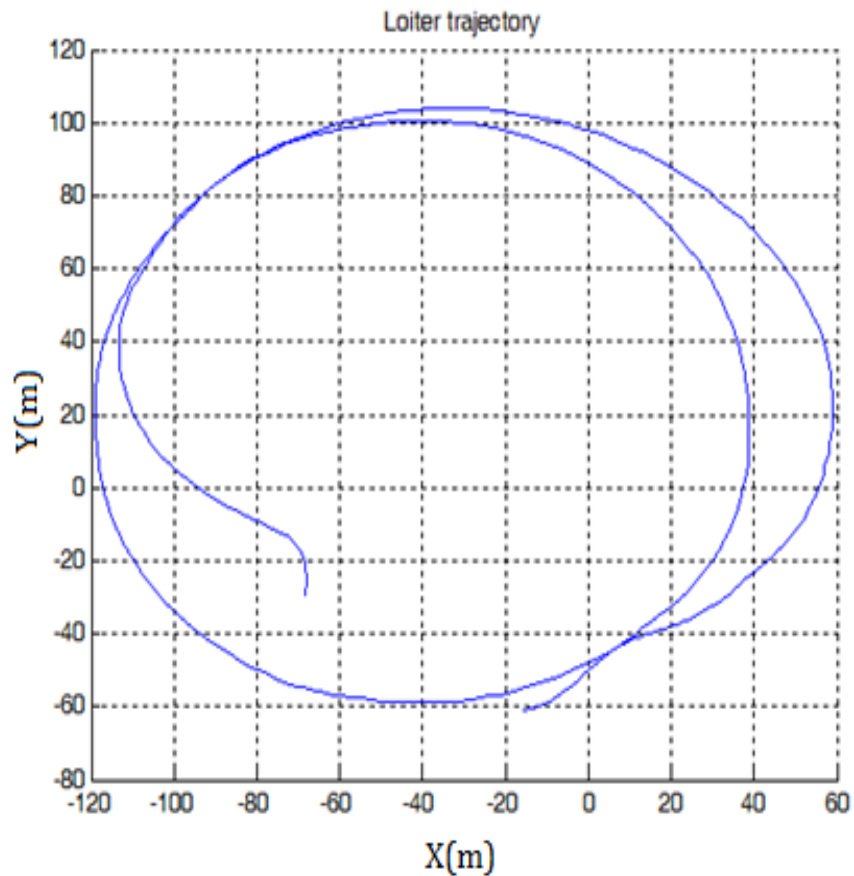


Fig. 4.14: Trajectory in loiter mode.

A second flight is shown in the following figures, this flight was with the same logic of the first one, where takeoff is done manually, then, the loiter mode is activated and after some turns, the landing is done manually.

In this flight is plotted not only the trajectory in two dimensions, but also the trajectory in three dimensions, as well as the altitude and speed during flight.

In the Fig. 4.15 is shown the loiter trajectory which describes around three turns, while in Fig. 4.16, the same trajectory is shown in 3D, where can be seen the complete behavior of the plane during the automatic flight.

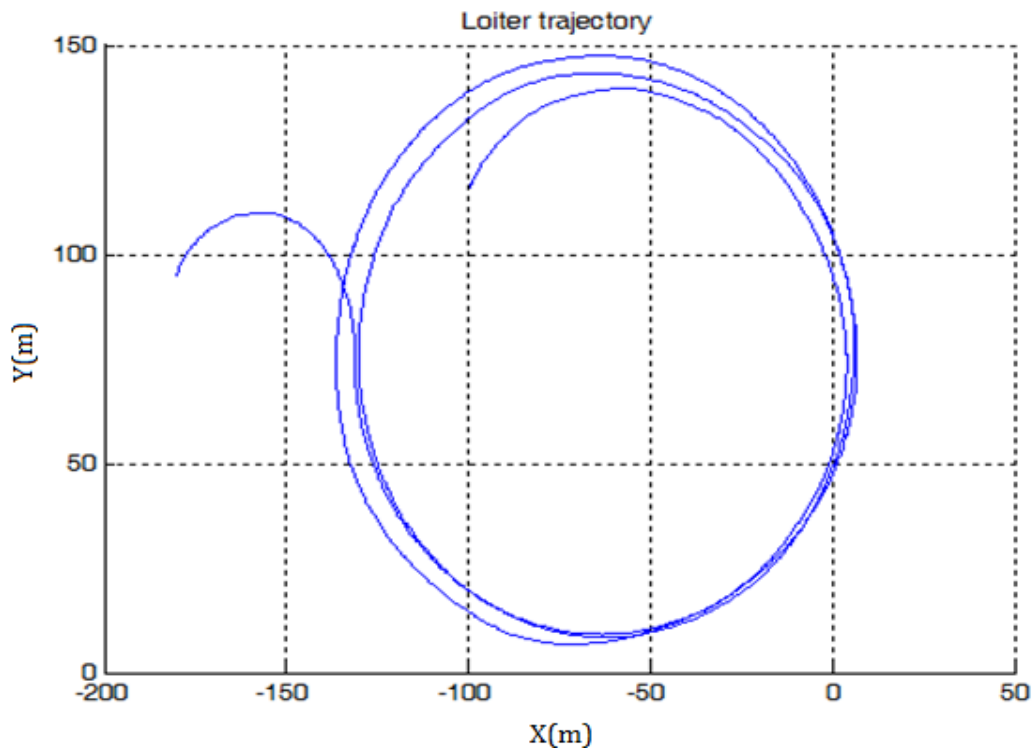


Fig. 4.15: Loiter trajectory.

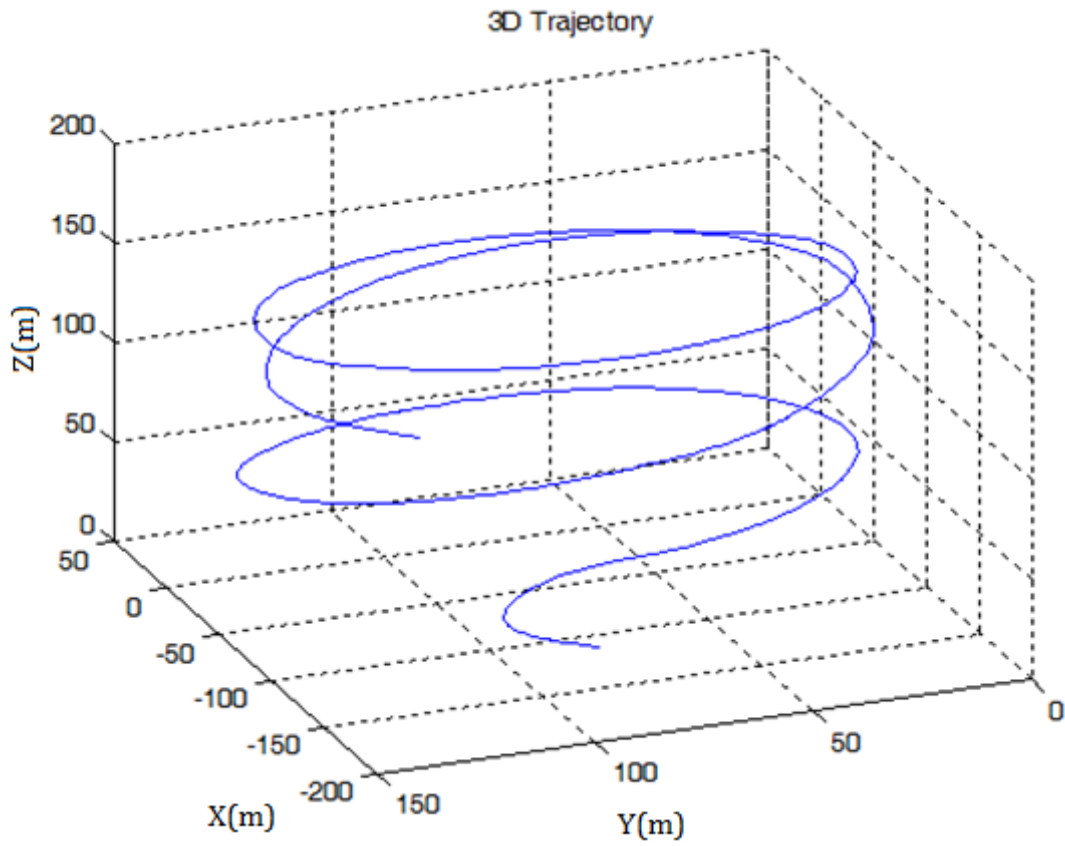


Fig. 4.16: 3D trajectory.

The altitude is shown closely in Fig. 4.17 aspect that complements the 3D trajectory and will serve to study the altitude control when this will be implemented.

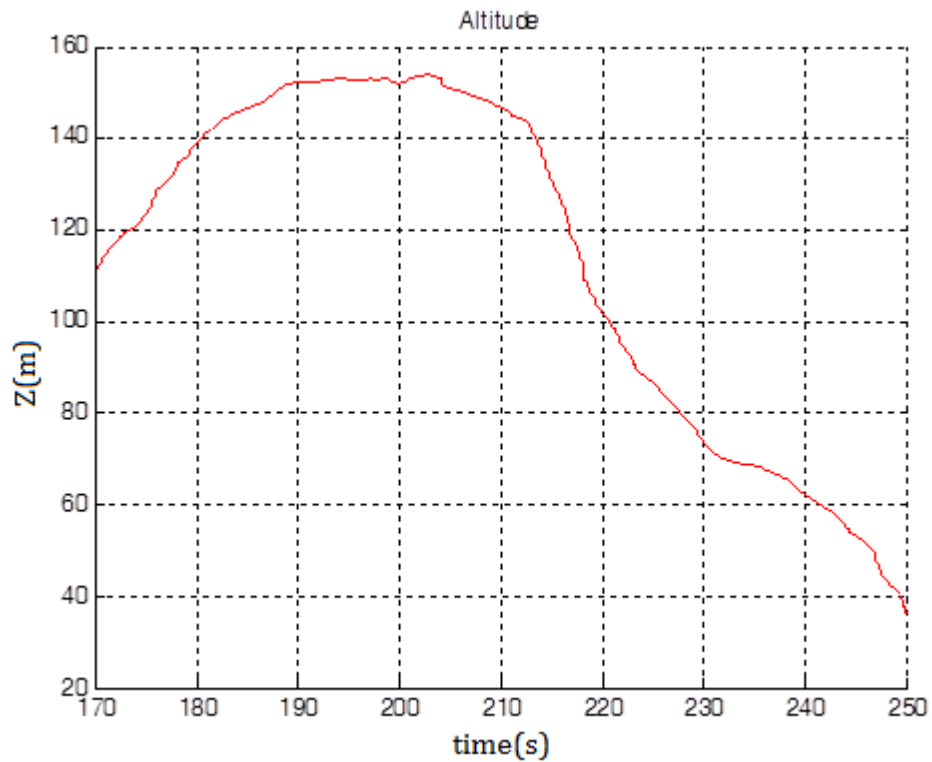


Fig. 4.17: Altitude during loiter flight.

The Fig. 4.18 shows the measures taken by the Pitot tube, which is the plane velocity relative to the air mass that surrounds it and must not be confused with the groundspeed, which is the plane velocity relative to the ground.

The magnitude of this physical quantity is closely related to the type of plane used, knowing its dependence on variables such as aerodynamic parameters, weight, propulsion, flight environment, endurance, and even the application wanted, just to mention some variables.

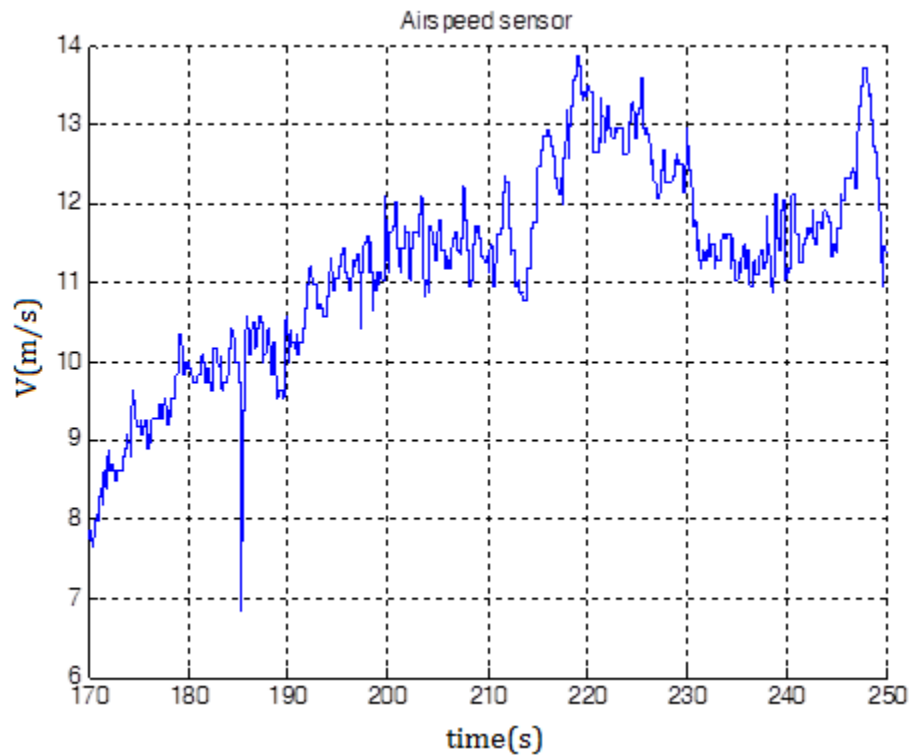


Fig. 4.18: Airspeed during partial flight.

If a better measure of the airspeed would have been sought, among all anemometers available in the market, the ones who give best approximations, included attack and sideslip angles estimates, are by far more expensive than a regular Pitot tube. For this work, economic materials are wanted, foreseeing possible crashes where all instrumentation can be lost.

The Fig. 4.19 shows part of the circular trajectory in order to show the accuracy of the algorithm. It can be appreciated that the starting point is almost the same as the final point of the path, but the radius of the path followed by the plane is not exactly the same as the commanded radius (65m), the time taken for the plane to perform the complete circle was about 25s.

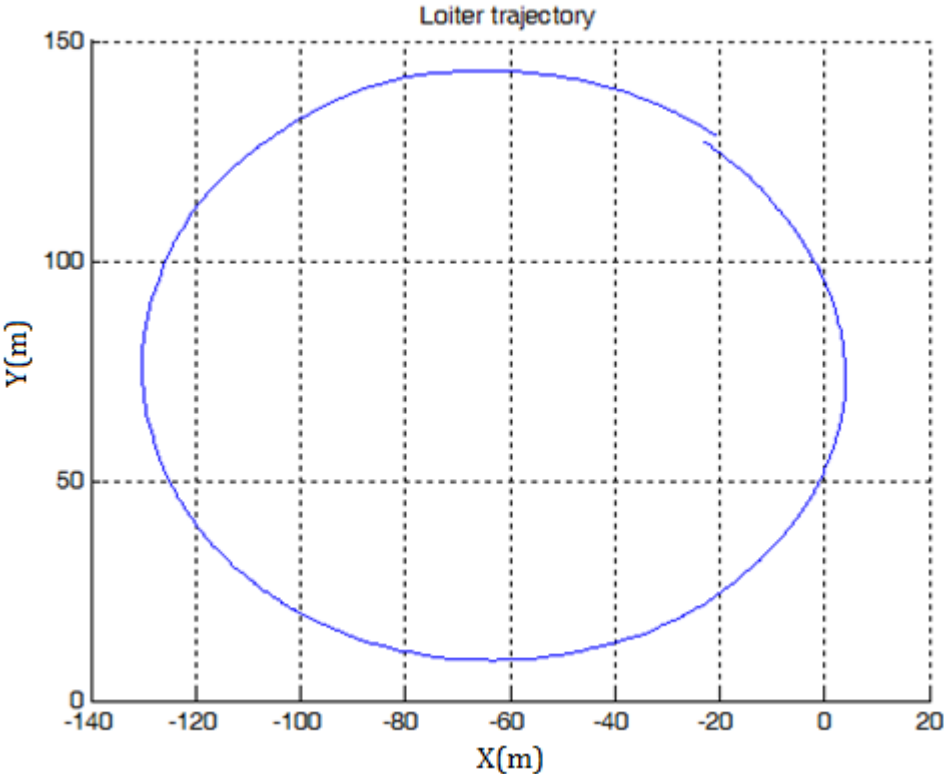


Fig. 4.19: Circular trajectory.

## **Discussion.**

Regarding to the algorithm used in the simulation to estimate wind disturbances, it can be also used to estimate non modeled plane dynamics or other aspects whose contributions could be taken as disturbances in general.

In the experimental results, being aware that the first approach of path following described in Chapter 2 is the one implemented, the accuracy of the method can be appreciated as the initial and final point of the trajectory are almost the same when the plane is performing one turn in the circular path following, but the radius of the path followed by the plane is not exactly the desired radius due to disturbances, leading to the possibility to improve these results using the second approach also described in Chapter 2, which is about to be implemented and compared in order to corroborate the robustness of the algorithm against wind gusts proven in theory.

During flights, two kinds of data management were done. The first management consisted on sending measurements through a wireless modem and visualize them in real time on a computer, the main problems with this management was that due to range bounds, or electromagnetic interference, data was modified or not received. The second data management was save all important variables measured into a SD card, in order to plot after flights these variables even if the data sent by the modem was unavailable. It is worth for saying that all economic wireless modems in the market are not enough good for plane applications due to the range bounds.

## **Conclusion.**

A method to ameliorate a carrot-chasing algorithm against wind disturbances is presented, showing to have a good performance in simulation when the wind estimates are combined with the path following control approach.

The wind estimation algorithm adds a delay in the signal to be estimated due to the processing time, this algorithm is easy to implement and enough accurate to the wanted purposes.

An experimental platform based on autopilot PX4 and economic sensors was developed in order to corroborate the proposed algorithm in this work, the materials and sensors are economic and easy replaceable due to the possibility of multiple crashes of the prototype.

In comparison with stationary flight prototypes as quad-copters, multicopters, coaxial-copters or any kind of helicopters, the experimental tests are by far, more difficult to perform in a plane, this is because a plane needs to have a relative velocity with respect to its surrounding mass in order to flight, translated into difficulties to adjust gains of controllers or solve “online” errors, and taking away big amounts of time repairing the platform when a crash is present.

The study of literature in aerodynamics, wind estimation, control laws, avionics, mathematical aspects, as well as the implementation and simulations of the approaches used, is well-founded.



## **Future Work.**

In order to hold up the results obtained in the second approach of path following presented in this work, the implementation in the real platform of the algorithm will be done. The platform that will be used has already been acquired, and an air data system has already been implemented to obtain real measurements of wind.

Moreover, after a revision of recent articles where the main issue is the wind treatment within a dynamic model in an aerial vehicle in general, it is a common constant the omission of the wind as a perturbation in the orientation; in almost all the works, wind is treated as a disturbance only in position, which in comparison with real facts, it's not as good as it could be if orientation dynamics could be disturbed by a term dependent on wind.

Furthermore, the expansion of the path following algorithm from two to three dimensions is wanted in order to not cope with the altitude separately.

According to the search of a lost person in the forest, a small camera with a vision algorithm capable to detect a person by any method would be ideal to close the loop.

## Appendix A.

### Lyapunov stability

Considering the nonlinear autonomus system

$$\dot{x} = f(x)$$

Where  $f: D \rightarrow \mathbb{R}^n$  is a locally Lipschitz (bounded by other function) map from a domain  $D \subset \mathbb{R}^n$  into  $\mathbb{R}^n$ . We suppose that the origin  $x = 0$  is an equilibrium point which satisfies:

$$f(0) = 0$$

It is said that the equilibrium point  $x = 0$  is:

- Stable, if for all  $\varepsilon > 0$ , there is a  $\delta = \delta(\varepsilon) > 0$  such that

$$\|x(0)\| < \delta \Rightarrow \|x(t)\| < \varepsilon, \quad \forall t \geq 0$$

- Unstable, if it is not stable
- Asymptotically stable, if it is stable and  $\delta$  can be chosen such that

$$\|x(0)\| < \delta \Rightarrow \lim_{t \rightarrow \infty} x(t) = 0$$

- Exponentially stable, if there exist two strictly positive numbers  $\alpha$  and  $\lambda$  independent of time and initial conditions such that

$$\|x(t)\| \leq \alpha \|x(0)\| e^{-\lambda t} \quad \forall t > 0$$

In some ball around the origin

The above definitions correspond to local properties of the system around the equilibrium point, this concepts will become global when their corresponding conditions are satisfied for any initial state.

### Lyapunov direct method

A scalar continuous function  $V(x)$  is said to be locally *positive (semi-) definite* if  $V(0) = 0$  and  $V(x) > 0$  ( $V(x) \geq 0$ ) for  $x \neq 0$ . Similarly,  $V(x)$  is said to be *negative (semi-) definite* if  $-V(x)$  is positive (semi-)definite.

$V(x)$  is called a *Lyapunov function* for the system if, in a ball  $B$  containing the origin,  $V(x)$  is positive definite and has continuous partial derivatives, and if its time derivative along the solution of the system is negative semi-definite, i.e.,  $\dot{V}(x) = \frac{\partial V}{\partial x} f(x) \leq 0$ .

**Theorem 1. (Local stability).** The equilibrium point of the system is locally (asymptotically) stable in a ball  $B$  if there exists a scalar function  $V(x)$  with continuous derivatives such that  $V(x)$  is positive definite and  $\dot{V}(x)$  is negative semi-definite (negative definite) in the ball  $B$ .

**Theorem 2. (Global stability).** The equilibrium point of the system is globally (asymptotically) stable if there exists a scalar function  $V(x)$  with continuous first order derivatives such that  $V(x)$  is positive definite,  $\dot{V}(x)$  is negative definite and  $V(x)$  is radially unbounded, i.e.,  $V(x) \rightarrow \infty$  as  $\|x\| \rightarrow \infty$ .

Krasovskii-LaSalle's invariant set theorem.

Krasovskii-LaSalle's results extend the stability analysis of the previous theorems when  $\dot{V}(x)$  is only negative semi-definite.

**Invariant set.** A set  $S$  is an invariant set for a dynamic system if every trajectory starting in  $S$  remains in  $S$ .

Invariant sets include equilibrium points, limit cycles as well as any trajectory of an autonomous system.

**Theorem 3. (LaSalle's invariance principle).** Let  $\Omega$  be a compact (closed and bounded) set with the property that every solution of the system which starts in  $\Omega$  remains in  $\Omega$  for all future time. Let  $V: \Omega \rightarrow \mathbb{R}$  be a continuously differentiable function such that

$\dot{V}(x) \leq 0$  in  $\Omega$ . Let  $E$  be the set of all points in  $\Omega$  where  $\dot{V}(x) = 0$ . Let  $M$  be the largest invariant set in  $E$ . Then every solution starting in  $\Omega$  approaches  $M$  as  $t \rightarrow \infty$ .

When  $V(x)$  is positive definite, the theorems 1 and 2 can be extended to these two corollaries:

Corollary 1. (Barbashin-LaSalle). Let  $x = 0$  be an equilibrium point of the system. Let  $V: D \rightarrow \mathbb{R}$  be a continuously differentiable positive definite function on a neighborhood  $D$  of  $x = 0$ , such that  $\dot{V}(x) \leq 0$  in  $D$ . Let  $S = \{x \in D | \dot{V}(x) = 0\}$ , and suppose that no solution can stay forever in  $S$ , other than the trivial solution. Then, the origin is asymptotically stable.

Corollary 2. (Krasovskii-LaSalle). Let  $x = 0$  be an equilibrium point of the system. Let  $V: \mathbb{R}^n \rightarrow \mathbb{R}$  be a continuously differentiable, radially unbounded, positive definite function such that  $\dot{V}(x) \leq 0$  for all  $x \in \mathbb{R}^n$ . Let  $S = \{x \in \mathbb{R}^n | \dot{V}(x) = 0\}$ , and suppose that no solution can stay forever in  $S$ , other than the trivial solution. Then, the origin is globally asymptotically stable.

When  $\dot{V}(x)$  is negative definite,  $S = \{0\}$ . Then, Corollaries 1 and 2 coincide with theorems 1 and 2 respectively.

## Appendix B.

In this appendix, will be showed how a lateral movement of a plane can be induced by a roll angle variation.

To understand this dynamic, the two types of Stability Derivatives, dimensional and non dimensional, are revised, according to the notation used in B. Etkin, “Dynamics of Flight”.

Knowing that the aerodynamic forces and moments depend on many time dependent variables, and also in their past state (for example, the vortex that is left behind the wing of a plane which induces a velocity field at the wing, changes the lift, so, strictly speaking, the lift not only depend on the instantaneous value of the attack angle, but also in its entire past history), it is better to express the aerodynamic forces and moments in terms of non dimensional coefficients.

The most common non dimensional coefficients are.

**The Nondimensional System**

(1)	(2)	(3)	
<i>Dimensional Quantity</i>	<i>Divisor— General Case</i>	<i>Divisor— Small- Disturbance Case</i>	
$X, Y, Z$	$\frac{1}{2}\rho V^2 S$	$\frac{1}{2}\rho V^2 S$	$C_x, C_y, C_z$
$mg$	$\frac{1}{2}\rho V^2 S$	$\frac{1}{2}\rho V^2 S$	
$M$	$\frac{1}{2}\rho V^2 S \bar{c}$	$\frac{1}{2}\rho V^2 S \bar{c}$	$C_m$
$L, N$	$\frac{1}{2}\rho V^2 S b$	$\frac{1}{2}\rho V^2 S b$	$C_l, C_n$
$u, v, w$	$V$	$u_0$	$\hat{u}, \hat{v}, \hat{w}$ (1)
$\alpha, q$	$2V/\bar{c}$	$2u_0/\bar{c}$	$\hat{\alpha}, \hat{q}$
$\beta, p, r$	$2V/b$	$2u_0/b$	$\hat{\beta}, \hat{p}, \hat{r}$
$m$	$\rho S \bar{c} / 2$	$\rho S \bar{c} / 2$	$\mu$
$I_y$	$\rho S (\bar{c} / 2)^3$	$\rho S (\bar{c} / 2)^3$	$\hat{I}_y$
$I_x, I_z, I_{xz}$	$\rho S (b / 2)^3$	$\rho S (b / 2)^3$	$\hat{I}_x, \hat{I}_z, \hat{I}_{xz}$
$t$	—	$t^* = \bar{c} / (2u_0)$	$\hat{t}$

Note: (1)  $\beta$  and  $\Delta\alpha$  are used interchangeably with  $\hat{\theta}$  and  $\hat{w}$ , respectively, in the small disturbance case.

The non dimensional derivatives express variations from the non dimensional coefficients with respect to other variables or coefficients, for example, the derivative:

$$C_{x_\alpha} = \frac{\partial C_x}{\partial \alpha} \Big|_{\alpha=0}$$

Express the change in the non dimensional coefficient  $C_x$ , ergo, in the aerodynamic force  $X$ , when the attack angle change.

The non dimensional derivatives are.

**Longitudinal Nondimensional Derivatives**

	$C_x$	$C_z$	$C_m$
$\hat{u}$	$C_{xu}$	$C_{zu}$	$C_{mu}$
$\alpha$	$C_{x\alpha}$	$C_{z\alpha}$	$C_{m\alpha}$
$\hat{q}$	$C_{xq}$	$C_{zq}$	$C_{mq}$
$\hat{\alpha}$	$C_{x\dot{\alpha}}$	$C_{z\dot{\alpha}}$	$C_{m\dot{\alpha}}$

**Lateral Nondimensional Derivatives**

	$C_y$	$C_l$	$C_n$
$\beta$	$C_{y\beta}$	$C_{l\beta}$	$C_{n\beta}$
$\hat{p}$	$C_{yp}$	$C_{lp}$	$C_{np}$
$\hat{r}$	$C_{yr}$	$C_{lr}$	$C_{nr}$
$\hat{\beta}$	$C_{y\dot{\beta}}$	$C_{l\dot{\beta}}$	$C_{n\dot{\beta}}$

In order to express de aerodynamic forces and moments more precisely under certain circumstances like atmospheric pressure constant in altitude, symmetric flight, etc., the dimensional stability derivatives which are dependent on the non dimensional stability derivatives are used, besides, the non dimensional stability derivatives relies on the non dimensional coefficients already defined.

So, the dimensional stability derivatives are.

**Longitudinal Dimensional Derivatives**

	$X$	$Z$	$M$
$u$	$\rho u_0 S C_{w_0} \sin \theta_0 + \frac{1}{2} \rho u_0 S C_{xu}$	$-\rho u_0 S C_{w_0} \cos \theta_0 + \frac{1}{2} \rho u_0 S C_{zu}$	$\frac{1}{2} \rho u_0 \bar{c} S C_{mu}$
$w$	$\frac{1}{2} \rho u_0 S C_{x\alpha}$	$\frac{1}{2} \rho u_0 S C_{z\alpha}$	$\frac{1}{2} \rho u_0 \bar{c} S C_{m\alpha}$
$q$	$\frac{1}{4} \rho u_0 \bar{c} S C_{xq}$	$\frac{1}{4} \rho u_0 \bar{c} S C_{zq}$	$\frac{1}{4} \rho u_0 \bar{c}^2 S C_{mq}$
$\dot{w}$	$\frac{1}{4} \rho \bar{c} S C_{x\dot{\alpha}}$	$\frac{1}{4} \rho \bar{c} S C_{z\dot{\alpha}}$	$\frac{1}{4} \rho \bar{c}^2 S C_{m\dot{\alpha}}$

**Lateral Dimensional Derivatives**

	$Y$	$L$	$N$
$v$	$\frac{1}{2} \rho u_0 S C_{y\beta}$	$\frac{1}{2} \rho u_0 b S C_{l\beta}$	$\frac{1}{2} \rho u_0 b S C_{n\beta}$
$p$	$\frac{1}{4} \rho u_0 b S C_{yp}$	$\frac{1}{4} \rho u_0 b^2 S C_{lp}$	$\frac{1}{4} \rho u_0 b^2 S C_{np}$
$r$	$\frac{1}{4} \rho u_0 b S C_{yr}$	$\frac{1}{4} \rho u_0 b^2 S C_{lr}$	$\frac{1}{4} \rho u_0 b^2 S C_{nr}$

Where the correct form to read the dimensional derivatives is, for example.

$$X_u = \frac{\partial X}{\partial u} |_{u=0}$$

Therefore, the aerodynamic forces and moments could be express like beyond, notice that the terms with subindex  $c$  are terms who denote the action of the control surfaces of the plane.

$$\begin{aligned}\Delta X &= X_u \Delta u + X_w w + \Delta X_c \\ \Delta Y &= Y_v v + Y_p p + Y_r r + \Delta Y_c \\ \Delta Z &= Z_u \Delta u + Z_w w + Z_{\dot{w}} \dot{w} + Z_q q + \Delta Z_c \\ \Delta L &= L_v v + L_p p + L_r r + \Delta L_c \\ \Delta M &= M_u \Delta u + M_w w + M_{\dot{w}} \dot{w} + M_q q + \Delta M_c \\ \Delta N &= N_v v + N_p p + N_r r + \Delta N_c\end{aligned}$$

### **The non dimensional derivative $C_{n_p}$**

The yawing and rolling motions are closely coupled, so that a rolling moment can produce a yawing motion and viceversa. The wing and tail both contribute.

The main wing contribution comes from the change in profile drag associated with the positive change in wing angle of attack. The wing  $\alpha$  is increased on the right-hand side and decreased on the left-hand side. These changes provoke an increase in profile drag on the right side, and decrease on the left side, combining to produce a positive (nose-right) yawing moment.

## References.

1. Bernard Etkin and Lloyd Duff Reid, "Dynamics of Flight, Stability and Control". New York, John Wiley & Sons, 1996.
2. Brian L. Stevens, Frank L. Lewis, "Aircraft Control and Simulation", John Wiley & Sons Inc, 1992.
3. Theodore Shifrin, "Differential Geometry: A First Course in Curves and Surfaces", University of Georgia, Spring, 2014.
4. S. Park, J. Deyst, J. P. How, "A New Nonlinear Guidance Logic for Trajectory Tracking", AIAA Guidance, Navigation and Control Conference, Massachusetts Institute of Technology, 2004.
5. P.B. Sujit, Srikanth Saripalli, and João Borges Sousa, "Unmanned Aerial Vehicle Path Following, A survey and analysis of algorithms for fixed-wing unmanned aerial vehicles", IEEE Control Systems Magazine, February 2014.
6. H. Chitsaz and S. LaValle, "Time-optimal paths for a dubins airplane." in Proc. IEEE Conference on Decision and Control (CDC'2007), New Orleans, LA, USA, Dec. 2007, pp. 2379–2384.
7. L. E. Dubins. "On curves of minimal length with a constraint on average curvature, and with prescribed initial and terminal positions and tangents", American Journal of Mathematics, 79:497–516, 1957.
8. Randal W. Beard, Timothy W. McLain, "Implementing Dubins Airplane Paths on Fixed-wing UAV", Springer Handbook for Unmanned Aerial Vehicles, Brigham Young University, July 2013.
9. S. Hota, D. Ghose, "A Modified Dubins Method for Optimal Path Planning of a Miniature Air Vehicle Converging to a Straight Line Path", American Control Conference, Hyatt Regency Riverfront, St. Louis, MO, USA, June 10-12, 2009.
10. A. Cho, J. Kim, S. Lee, "Wind Estimation and Airspeed Calibration using a UAV with a Single-Antenna GPS Receiver and Pitot Tube", IEEE Transactions on aerospace and electronic systems, vol. 47, no. 1, January 2011.



11. M. Rhudy, T. Larrabee, et al., "UAV Attitude ,Heading, and Wind Estimation Using GPS/INS and an Air Data System", American Institute of Aeronautics and Astronautics (AIAA) Guidance, Navigation, and Control (GNC) Conference, Boston, Ma, August 19-22, 2013.
12. C. Liu, O. McAree, W. Chen, "Path-following control for small fixed-wing unmanned aerial vehicles under wind disturbances", International Journal of Robust and Nonlinear Control 2013, 23:1682-1698.
13. J. Langelaan, N. Alley, J. Neidhoefer, "Wind field estimation for small unmanned aerial vehicles", AIAA Guidance, Navigation and Control Conference, Toronto, Canada, 2010.
14. J. Langelaan, J. Spletzer, C. Montella, J. Grenestedt, "Wind field estimation for autonomus dynamic soaring", 2012 IEEE International Conference on Robotics and Automation, RiverCentre, Saint Paul, Minnesota, USA, May 14-18, 2012.
15. A. Brezoescu, T. Espinoza, P. Castillo, R. Lozano, "Adaptive Trajectory Following for a Fixed-Wing UAV in Presence of Crosswind", Journal of Intelligent and Robotic Systems 69, January 2013.
16. A. Brezoescu, P. Castillo, R. Lozano, "Wind estimation for accurate airplane path following applications", 2013 International Conference on Unmanned Aircraft Systems (ICUAS), Grand Hyatt Atlanta, Atlanta, GA, May 28-31, 2013, pp. 869-874.
17. D. Nelson, D. Barber, T. McLain, "Vector field path following for miniature air vehicles", IEEE Transactions on Robotics, vol. 23, no. 3, June 2007.
18. Alain Micaelli, Claude Samson, "Trajectory tracking for unicycle-type and two-steering-wheels mobile robots", Institut National de Recherche en Informatique et en Automatique, Rapport de Recherche, November 1993.
19. L. Lapierre and D. Soetanto, "Nonlinear path-following control of an AUV", Ocean Engineering, vol. 1112, no. 34, p. 1734-1744, 2007.
20. G. Flores, I. Lugo-Cardenas, and R. Lozano, "A nonlinear path-following strategy for a fixed-wing mav", in 2013 International Conference on Unmanned Aircraft Systems (ICUAS), Grand Hyatt Atlanta, Atlanta, GA, May 28-31, 2013, pp. 1014-1021.

21. A. Levant, "Higher-order sliding modes, differentiation and output-feedback control", International Journal of Control, vol. 76, p. 924-941, 2003.
22. Hassan K. Khalil. "Nonlinear Systems, third edition", Prentice Hall, 128pp.
23. Lorenz Meier, Dominik Honegger and Marc Pollefeys. "PX4: A Node-Based Multithreaded Open Source Robotics Framework for Deeply Embedded Platforms", International Conference on Robotics and Automation (ICRA) 2015.
24. J. P. Snyder, "Map Projections a Working Manual", U.S. Geological Survey Professional Paper 1395, 164-168pp.
25. Lorenz Meier, <http://qgroundcontrol.org/>, 2009